https://doi.org/10.5194/egusphere-2023-1564
Preprint. Discussion started: 13 July 2023

Surface factors controlling the volume of accumulated Labrador Sea Water

Yavor Kostov[1,2], Marie-José Messias[1], Herlé Mercier[3], David P. Marshall[4], Helen L. Johnson[5]

[1]U. of Exeter, Department of Geography, Exeter, United Kingdom
[2]British Antarctic Survey, Cambridge, United Kingdom
[3]U. of Brest, Laboratoire d'Océanographie Physique et Spatiale, CNRS, Brest, France
[4]U. of Oxford, Department of Physics, Oxford, United Kingdom
[5]U. of Oxford, Department of Earth Sciences, Oxford, United Kingdom

Correspondence to: Yavor Kostov (yastov@bas.ac.uk)

Abstract. We explore historical variability in the volume of Labrador Sea Water (LSW) using ECCO, an ocean state estimate configuration of the Massachusetts Institute of Technology general circulation model (MITgcm). The model's adjoint, a linearization of the MITgcm, is set up to output the lagged sensitivity of the watermass volume to surface boundary conditions. This allows us to reconstruct the evolution of LSW volume over recent decades using historical surface wind stress, heat, and freshwater fluxes. Each of these boundary conditions contributes significantly to the LSW variability that we recover, but these impacts are associated with different geographical fingerprints and arise over a range of time lags. We show that the volume of LSW accumulated in the Labrador Sea exhibits a delayed response to surface wind stress and buoyancy forcing outside the convective interior of the Labrador Sea, at key locations in the North Atlantic Ocean. In particular, winds and surface density anomalies affect the North Atlantic Current's (NAC) transport of warm and saline subtropical water masses that are precursors for the formation of LSW. This propensity for a delayed response of LSW to remote forcing allows us to predict a substantial fraction of LSW variability at least a year into the future. Our analysis also enables us to attribute LSW variability to different boundary conditions and to gain insight into the major mechanisms that drive volume anomalies in this deep watermass. We point out the important role of buoyancy loss and preconditioning along the NAC pathway, in the Iceland Basin, the Irminger Sea, and the Nordic Seas, processes which facilitate the formation of LSW both in the Irminger and in the Labrador Sea.

1. Introduction

Labrador Sea Water (LSW) is a deep watermass that forms during episodes of intense wintertime convection in the Labrador and Irminger Seas (e.g., Pickart et al., 2003a). LSW plays an important role in the decadal and multidecadal variability of the Atlantic Meridional Overturning Circulation (AMOC) (Yeager et al, 2021; Oldenburg et al. 2021), while the connection between LSW and AMOC variability on shorter timescales is unclear (Li et al, 2019). In addition, LSW contributes significantly to the ocean uptake and storage of heat (Desbruyeres et al., 2014; Messias and Mercier, 2022) and tracers such as carbon and oxygen (Terenzi et al., 2007; Perez et al., 2013; Rhein et al., 2017; Koelling et al. 2022), which can affect the pace of regional and global climate change.

https://doi.org/10.5194/egusphere-2023-1564
Preprint. Discussion started: 13 July 2023

The volume budget of LSW in the Labrador Sea is a complex balance between multiple mechanisms that are at play throughout different seasons. In the winter, deep convection in the subpolar North Atlantic depends on a set of prerequisites that pre-condition vertical instability of the water column in the Labrador or Irminger Seas (Pickart et al. 2003a). One of these necessary conditions is the availability of weakly-stratified Subpolar Mode Water, which forms in the eastern subpolar gyre and is a precursor that can get transformed into LSW (Petit et al 2020; Brambilla et al. 2008; Talley and McCartney 1982).

In models and observations, a fraction of the LSW produced during wintertime convective events in the Labrador Sea is exported to the subtropical gyre both along the Deep Western Boundary Current and along interior pathways (Lozier et al., 2012) while the remainder recirculates within the subpolar gyre. The relationship between LSW production and export is complex (Zou and Lozier, 2016) because the subpolar gyre stores a large volume of LSW formed over a range of years (Zou and Lozier, 2016). LSW recirculates between the Labrador Sea, the Iceland Basin, and the Irminger Sea (Yashayaev et al., 2007a). In addition, some LSW is formed in the Irminger Sea (Pickart et al. 2003a; Pickart et al. 2003b). Export and recirculation are not the only processes that deplete the volume of LSW in the Labrador Sea. Once LSW is isolated from the ocean's surface mixed layer, it experiences restratification and mixes with other water masses via isopycnal stirring (Lazier et al., 2002; Yashayaev 2007b). General circulation models tend to overestimate the seasonal depletion of LSW (Li et al., 2019) and hence underestimate the fraction of LSW stored in the Labrador Sea from one year to another.

The time-mean, the seasonal cycle, and the anomalies in LSW volume in the Labrador Sea (Fig. 1a) of the ECCO state estimate (Forget et al., 2015), used in this study, are on the order of $10^{14}\ m^3$ (Fig. 1b), which is similar to basin-wide observations (Li et al., 2019). The annual mean volume of LSW and the anomalies relative to the seasonal mean are on the same order of magnitude, which gives rise to a very fluctuating timeseries of historical watermass variability (Fig. 1b). The ECCO state estimate consistently reproduces historical LSW variability such as the 2008 rise in watermass volume (Yashayaev and Loder, 2009).

There are various approaches for estimating watermass budgets using data from observations or reanalysis products, and some of these methods have been successfully applied to LSW. Mackay et al. (2020) use the Regional Thermohaline Inverse Method (Mackay et al., 2018) to estimate the formation, export, and mixing of LSW. Li et al. (2019) use observational Argo float data to calculate LSW volume over the Labrador Sea. Other studies rely on section-based data for LSW layer thickness to estimate watermass volume changes over the whole basin (Yashayaev and Loder, 2009; Rhein et al., 2017). Here we present a different method whose advantage is that we use only surface boundary conditions to reconstruct LSW volume variability. In addition, our approach allows us to obtain limited predictability of LSW volume anomalies a year into the future.

In our method, we use the adjoint of the Massachusetts Institute of Technology general circulation model (MITgcm), a linearization of the model, to estimate the lagged linear sensitivity of LSW volume in the Labrador Sea to surface wind stress, as well as surface fluxes of heat and freshwater. A number of previous studies have applied the adjoint of the MITgcm to exploring sources of ocean variability (e.g., Heimbach et al, 2011; Pillar et al., 2016; Jones et al., 2018; Smith and Heimbach, 2019; Kostov et al. 2021; Boland et al. 2021; Kostov et al., 2022), but we are the first to use this framework for reconstructing variability in the volume of LSW accumulated in the Labrador Sea. In addition, our method allows us to attribute historical

https://doi.org/10.5194/egusphere-2023-1564
Preprint. Discussion started: 13 July 2023

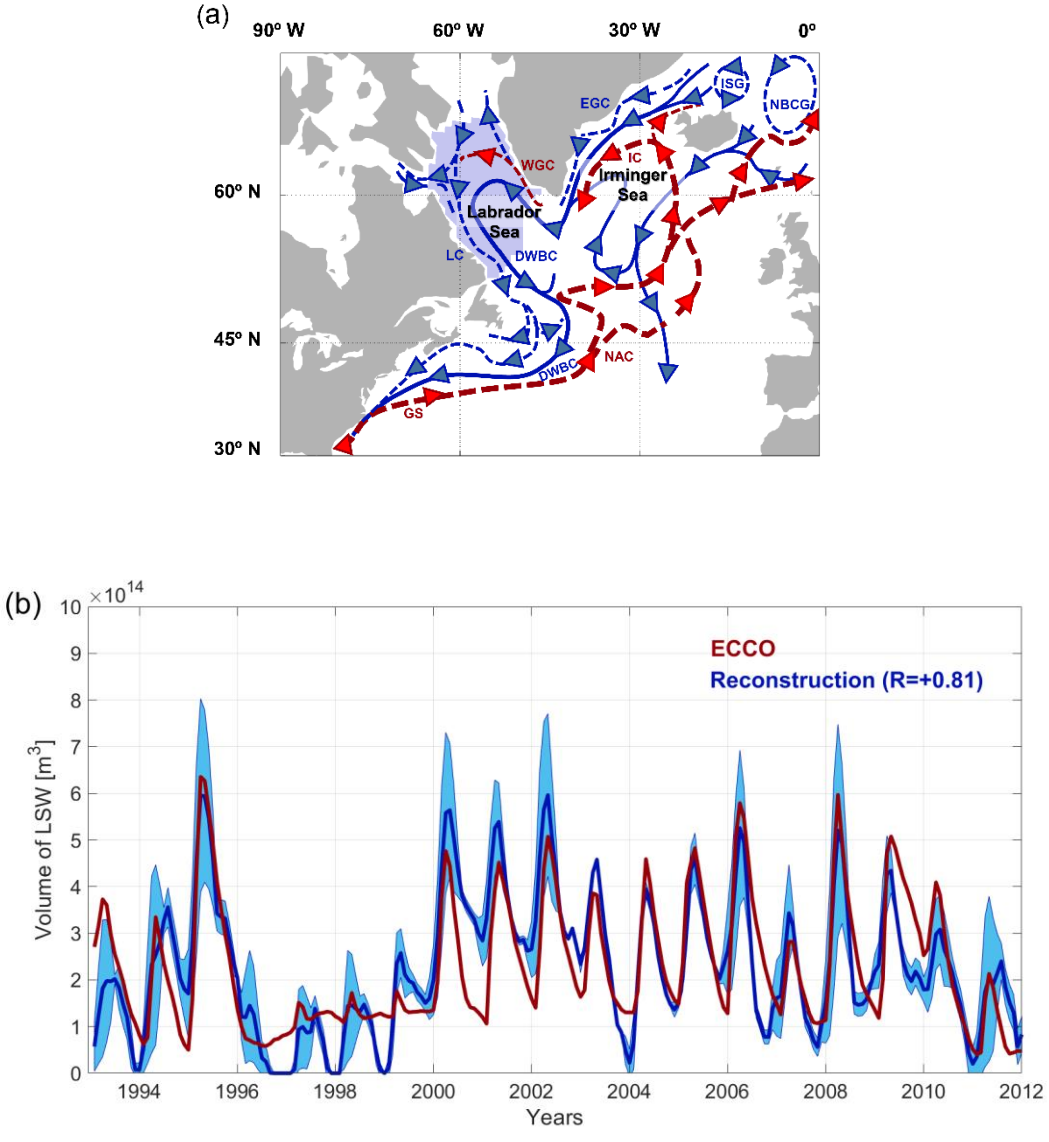

Figure 1: (a) Spatial mask (light purple shading) of the Labrador Sea region where we calculate the volume of stored LSW. The region is bounded by the OSNAP-West array in the southeast (Lozier et al., 2017). The continental base mask is generated using the free and publicly available software "M_Map: A mapping package for MATLAB", provided by R. Pawlowicz. Superimposed is a schematic of the high-latitude circulation in the North Atlantic ocean following Våge et al. (2013), Houpert et al. (2018), Raj et al. (2019), Florindo-López et al. (2020), and Jutras et al. (2023). Dashed curves represent surface currents, and solid curves deep currents with the direction indicated by arrows. Blue and red denote the transport of relatively cold and warm water, respectively. The thicker curves correspond to relatively larger volume transport. Labels denote: GS (Gulf Stream); DWBC (Deep Western Boundary Current); NAC (North Atlantic Current); LC (Labrador Current); WGC (West Greenland Current); IC (Irminger Current); EGC (East Greenland Current); ISG (Iceland Sea Gyre) ; NBCG (Norwegian Basin Cyclonic Gyre circulation). (b) Monthly-mean timeseries of LSW volume [m^3] in the ECCO state estimate (red) and in our monthly-average reconstruction (dark blue line), which includes recovered monthly anomalies and the ECCO climatological seasonal cycle. The reconstructed LSW volume is set to be strictly nonnegative at the end of 1996, 1997, and 1999. Blue shading reflects the uncertainty in the mean estimate approximated as the difference between the minimum and the maximum of the three different reconstructions at each point in time.

https://doi.org/10.5194/egusphere-2023-1564
Preprint. Discussion started: 13 July 2023

watermass anomalies to different surface boundary conditions and to identify some of the physical mechanisms that govern the LSW volume budget.

In Section 2 we describe our methods for estimating the watermass volume budget using surface boundary conditions. In Section 3, we analyze our results and compare them to observations. In Section 4, we discuss the wider implications of our findings and their relevance to physical processes in the North Atlantic subpolar gyre.

2. Methods

2.1 General circulation model and its algorithmic differentiation

The state-of-the-art Massachusetts Institute of Technology general circulation model (MITgcm) has been successfully applied in many studies exploring ocean dynamics on regional and global scales (Marshall et al. 1997). Here we use ECCO, a special configuration of the MITgcm: an ocean state estimate, in which the model is fit to available observations in a least squared sense (Forget et al. 2015).

One of the most advanced features of the MITgcm is that the model code is automatically differentiable (Giering, 2010), which allows for the generation of an adjoint linearization (Heimbach et al., 2011; Fukumori et al., 2017; Marotzke et al, 1999; Forget et al., 2015). This capability is essential for the development of the ECCO ocean state estimate (Fukumori et al., 2017; Forget et al., 2015). The adjoint of the model outputs the linear sensitivity (first derivatives) of a specified ocean index, an objective function, with respect to parameter choices and different boundary conditions over a range of lead times.

2.2 Objective Function

In this work, our objective function of interest is the volume of LSW in the Labrador Sea region (Fig. 1a), bounded by the OSNAP-West line (Lozier et al., 2017). We define LSW using a combination of two criteria. The first criterion sets bounds on the potential density σ_θ of the watermass referenced to the surface:

$$\sigma_{\theta\ lower} < \sigma_\theta < \sigma_{\theta\ upper} \quad (1)$$

where $\sigma_{\theta\ lower} = 27.7\text{kg m}^{-3}$ and $\sigma_{\theta\ upper} = 27.84\ \text{kg m}^{-3}$. This condition ensures that the watermass we consider is in the density range of Upper North Atlantic Deep Water (Zou and Lozier, 2016; Li et al., 2019), whose density structure is realistically represented in the ECCO state estimate. The second criterion is defined in terms of potential vorticity (PV),

$$\text{PV} < \text{PV}_{\text{upper}} \quad (2)$$

where the upper bound $\text{PV}_{\text{upper}} = 4 \times 10^{-12} m^{-1} s^{-1}$ as in Zou and Lozier (2016). Following Zou and Lozier, (2016) we approximate PV in terms of the vertical stratification:

$$PV \approx f \frac{N^2}{g} \quad (3)$$

where f is the Coriolis parameter, g is the gravitational acceleration, and N is the buoyancy frequency. Thus, the PV condition which we impose ensures that we define LSW as a weakly stratified watermass.

https://doi.org/10.5194/egusphere-2023-1564
Preprint. Discussion started: 13 July 2023

We formulate our objective function for the volume of LSW in the Labrador Sea (Vol) such that it is continuously differentiable by the algorithmic differentiation software (Giering, 2010). We therefore impose the PV and potential density criteria (Eq. (1) and (2)) by using logistic activation functions $A(a,b)$ of the form

$$A(a,b) = (1/2 + \tanh((a-b)\,c)/2) \tag{4}$$

that approximate the Boolean conditions of the form $a > b$ in our definition of LSW (e.g., Fig. A1 in the Appendix A). Our objective function is thus defined as:

$$\begin{aligned} Vol \;=\; & \frac{1}{(t_{end}-t_0)} \sum_{t_0}^{t_{end}} \sum_{x,y,z} GridCellVolume(x,y,z) \\ & \cdot A(\sigma_\theta(x,y,z,t), \sigma_{theta\ lower}) \\ & \cdot \left(1 - A\left(\sigma_\theta(x,y,z,t), \sigma_{theta\ upper}\right)\right) \\ & \cdot (1 - A\left(PV(x,y,z,t), PV_{upper}\right)) \\ & \cdot A(PV(x,y,z,t), -1000) \end{aligned} \tag{5}$$

where $c = 10^5\ kg^{-1}\ m^3$ or $c = 10^5\ m\ s$ is a factor that controls the slope of the activation function with respect to the input, and $GridCellVolume$ is the volume of each grid cell. The last factor in our formula includes a lower bound on $PV > -1000 \times 10^{-12} m^{-1} s^{-1}$, which in practice is always satisfied and includes vertically unstable water columns in the Labrador Sea. For a discussion of the activation functions, see Appendix A and Fig. A1 and A2. The right hand side of Eq. (5) is summed over the model's horizontal x, y and depth (z) coordinates within the Labrador Sea region bounded by the OSNAP-West line (Lozier et al., 2017) to the southeast (Fig. 1a). The objective function is furthermore averaged in time over a simulated time interval $t_{end} - t_0$ which is equal to 1 month.

Our objective function, LSW volume, has values on the order of $10^{14}\ m^3$ and exhibits variability on the same order of magnitude. However, we do not compute the objective function in units of $10^{14}\ m^3$. Instead, we rescale the LSW volume by a large nondimensional factor of 1500. This rescaling eliminates some of the numerical noise that arises when the adjoint of the MITgcm outputs the sensitivity of our objective function to surface boundary conditions. We then divide the lagged sensitivity patterns by 1500 when we post-process them offline.

The value of our objective function and its sensitivity to boundary conditions depends on the season in which we measure the objective function. The sensitivity of winter LSW volume to past surface boundary conditions is different from the sensitivity of summer LSW volume. However, computing the sensitivity of objective functions evaluated over each calendar month is too computationally expensive. Instead, as in Kostov et al. (2021), we conduct 4 adjoint calculations where the objective function is evaluated over four different representative months of the year, corresponding to spring, summer, fall, and winter seasons during the 2006-2007 historical period. In addition, for comparison, we do two more adjoint calculations

https://doi.org/10.5194/egusphere-2023-1564
Preprint. Discussion started: 13 July 2023

with winter objective functions computed in March 2006 and March 2011. The years 2006, 2007, and 2011 represent diverse regimes of the North Atlantic Oscillation (Fig. B1), which is among the major drivers of ocean variability in the North Atlantic subpolar gyre (Roussenov et al., 2022). These three years are also marked by different winter mixed layer depths in the Labrador Sea and different volume of LSW in the background ocean state (Fig. B1).

2.3 Using lagged sensitivity to reconstruct and attribute variability

When we define the LSW volume Vol as our objective function, we compute its linear sensitivity S with respect to surface boundary conditions. For example, we consider surface heat fluxes Q at geographical location $\boldsymbol{x}$ and at a lead time t_{lead} and compute the sensitivity

$$S(Q, \boldsymbol{x}, \tau) = \frac{\partial Vol}{\partial Q(\boldsymbol{x}, t_{lead})} \quad (6)$$

in units of $[m^3\ per\ W^{-1}m^2]$. For each lead time t_{lead}, the adjoint of the model produces spatial maps that show the sensitivity of the LSW volume to surface heat fluxes. They tell us whether warming or cooling part of the ocean surface causes a delayed increase or decrease in the volume of the watermass. Similarly, we obtain analogous sensitivity maps with respect to surface freshwater fluxes F, and zonal and meridional wind stress τ_N, τ_E.

The linear sensitivity patterns generated by the adjoint can be used to reconstruct and attribute variability in the objective function of interest, in our case, LSW volume. We convolve the lagged sensitivity to each surface boundary condition B with the time-history of anomalies in that boundary condition over a range of lead times t_{lead}. We repeat the same approach for heat and freshwater fluxes, as well as surface winds,

$$Vol(t) \approx \sum_{B=Q,F,\tau_N,\tau_E} \int_0^{t_{cutoff}} \int S(B, \boldsymbol{x}, t_{lead})\, B(t - t_{lead})\, d\boldsymbol{x}\, dt_{lead} \quad (7)$$

to recover a timeseries of the anomalies in watermass volume $Vol(t)$. We use this method to estimate variability of LSW relative to the seasonal or annual mean watermass volume. For practical purposes, in our study, we choose a maximum cut-off lead-time $t_{cutoff} = 6.5\ years$ beyond which we assume no memory of past surface forcing (See Fig. C1 and the discussion in Appendix C). By using sensitivity patterns from winter objective functions evaluated in 2006, 2007, and 2011, we obtain three different reconstructions. Looking at the difference between the minimum and the maximum of these reconstructions at each point in time gives us a rough estimate of the uncertainty due to linearizing the model simulation over particular historical periods with different background states of the ocean.

If surface forcing at lead-times greater than zero contributes significantly to the reconstruction of LSW volume variability, we can use this information to make predictions about future anomalies in $Vol(t)$ over a time horizon $t_{horizon}$:

$$Vol_{prediction}(t) = \sum_{B=Q,F,\tau_N,\tau_E} \int_{t_{horizon}}^{t_{cutoff}} \int S(B, \boldsymbol{x}, t_{lead})\, B(t - t_{lead})\, d\boldsymbol{x}\, dt_{lead} \quad (8)$$

In addition to reconstructing and predicting variability, this approach can also be used for causal attribution. We can decompose the reconstruction in Eq. (7) into separate contributions by wind stress, heat, and freshwater fluxes at the surface. This allows us to highlight the individual roles of these different sources of variability.

https://doi.org/10.5194/egusphere-2023-1564
Preprint. Discussion started: 13 July 2023

The default sensitivity patterns calculated by the adjoint contain built-in information about air-sea feedback represented using bulk formulae and a parameterization of surface radiation. For example, the default sensitivity patterns assume that anomalous shortwave heat flux into the ocean subsequently triggers a combination of radiative cooling, evaporation, and/or turbulent heat flux out of the ocean (Kostov et al., 2019). This response of the ocean is also part of the net surface heat flux budget. Therefore, both the net surface heat fluxes Q and the default sensitivity patterns $S(Q, x, t - t_{lead})$ output by the adjoint include air-sea feedback. As a result, the convolution in Eq. (7) can erroneously double count air-sea feedback mechanisms.

In order to avoid this problem, we cannot rely on the default configuration of the adjoint. Instead, we have to instruct the algorithmic differentiation software not to take derivatives of the bulk formulae and the surface radiation parameterization code. This approach guarantees that our lagged sensitivity patterns do not include air-sea feedback effects that are already accounted for in the net surface heat flux budget.

2.4 Identification of preferred lead times in the ocean system

We can use our linear convolution framework to gain additional insight into the lead-lag relationships between surface boundary conditions in different regions and the volume of LSW. In other words, we can identify if surface boundary conditions in certain geographical regions have preferred lead times at which they drive LSW volume anomalies. For example, we can look at different lead times t_{lead} and compute the contribution that surface heat fluxes Q over a particular region make at each of these lead times:

$$Vol_Q(t, t_{lead}, \boldsymbol{X}) = \int S(Q, \boldsymbol{x}, t_{lead}) Q(t - t_{lead})\, \boldsymbol{X}(\boldsymbol{x})\, d\boldsymbol{x} \quad (9)$$

where $\boldsymbol{X}(\boldsymbol{x})$ is a regional spatial mask set to 1 in the region of interest and 0 everywhere else.

We consider the Pearson correlation R between $Vol_Q(t, t_{lead}, \boldsymbol{X})$ for each lead time $t_{lead} = T$ on one hand, and the sum over all lead times $\sum_{t_{lead}} Vol_Q(t, t_{lead}, \boldsymbol{X})$ for a given region $\boldsymbol{X}$:

$$R(T) = R\left[Vol_Q(t, t_{lead} = T, \boldsymbol{X}), \sum_{t_{lead}} Vol_Q(t, t_{lead}, \boldsymbol{X})\right] \quad (10)$$

However, the Pearson correlation does not give us an idea about the *magnitude* of variability at each lead time that projects onto the regional contribution of a particular boundary condition to LSW anomalies. To estimate this magnitude in units of m^3, we can weight $R(T)$ from Eq. (10) by the standard deviation of $Vol_Q(t, t_{lead} = T)$:

$$R(T)\, std\left(Vol_Q(t, t_{lead} = T, \boldsymbol{X})\right) \quad (11)$$

Peak values of the weighted lagged correlation (Eq. (11)) with respect to t_{lead} indicate characteristic or preferred lead times at which a given geographical region $\boldsymbol{X}$ contributes to LSW volume variability.

2.5 Identification of key geographical regions and major processes as sources of remote influence on LSW volume anomalies

In addition to identifying preferred lead times in the system, we can use the sensitivity patterns S generated by the adjoint to identify the most important regions of the ocean that exert a delayed impact on the volume budget of LSW. The

https://doi.org/10.5194/egusphere-2023-1564
Preprint. Discussion started: 13 July 2023

patterns S represent the hypothetical proclivity of LSW to respond to surface boundary conditions. However, there has to be actual variability in these surface boundary conditions to activate the sensitivity patterns. Therefore, we are interested in how variability in each surface boundary condition projects on the spatial sensitivity patterns at different lead times. For example, we may consider maps of the standard deviation of net surface heat fluxes $std_Q(\boldsymbol{x})$ and use these to weight $S(Q, \boldsymbol{x}, t_{lead})$ pointwise at each model grid cell:

$$std_Q(\boldsymbol{x}) \cdot S(Q, \boldsymbol{x}, t_{lead}) \quad (12)$$

These projections highlight the geographical regions that make the largest delayed contributions to LSW variability. For instance, Eq. (12) can identify parts of the ocean where surface heat fluxes tend to trigger LSW volume anomalies at a lead time t_{lead}.

In order to understand the physical processes that relate surface boundary conditions to delayed responses in the LSW budget, we combine our adjoint calculations with forward perturbation experiments, as follows. We take the sensitivity to surface freshwater fluxes F at a given lead-time $S(F, \boldsymbol{x}, t_{lead})$ and apply this spatial pattern as a perturbation to the freshwater flux field $F(\boldsymbol{x})$ in the model:

$$F_{perturbed}(\boldsymbol{x}) = F(\boldsymbol{x}) + \mu \cdot S(F, \boldsymbol{x}, t_{lead}) \quad (13)$$

where μ is a scaling constant. The results of such a perturbation experiment, relative to the unperturbed simulation, reveal what physical mechanisms are activated on different timescales when boundary conditions project onto the sensitivity pattern S.

3. Results

Using the time-history of surface wind-stress, heat flux, and freshwater flux, along with sensitivity patterns generated by the MITgcm adjoint, we reconstruct monthly-averaged timeseries of the LSW volume anomalies relative to each month of the seasonal cycle (Eq. (7)). We then add our reconstructed anomalies to the climatological seasonal cycle from ECCO and compare the sum with historical LSW variability in the state estimate. Linearizing the model over different time periods allows us to produce three different sets of sensitivity patterns and hence, three different historical reconstructions. This ensemble gives us an envelope of uncertainty which reflects the importance of the background ocean state for the response of LSW to surface boundary conditions (shading in Fig. 1b). We point out that individual reconstructions generally agree on the sign of the LSW volume anomalies but differ in the estimated magnitude of the anomalies with large uncertainty, on the order of $10^{14}\ m^3$. Overall, the magnitude of reconstructed LSW volume variability is consistent with the observational estimates of Li et al. (2019).

Our ensemble-mean result reproduces relatively well (R=+0.81) the ECCO timeseries of watermass volume (Fig. 1b) except for certain episodic mismatches, e.g., during some of the winter months and over the 1996-1999 period marked by low LSW accumulation in the Labrador Sea. Our reconstruction markedly underestimates the LSW volume in the second half of 1996 and even reaches unrealistic values: we have to impose a separate condition that the total LSW volume in the Labrador

https://doi.org/10.5194/egusphere-2023-1564
Preprint. Discussion started: 13 July 2023

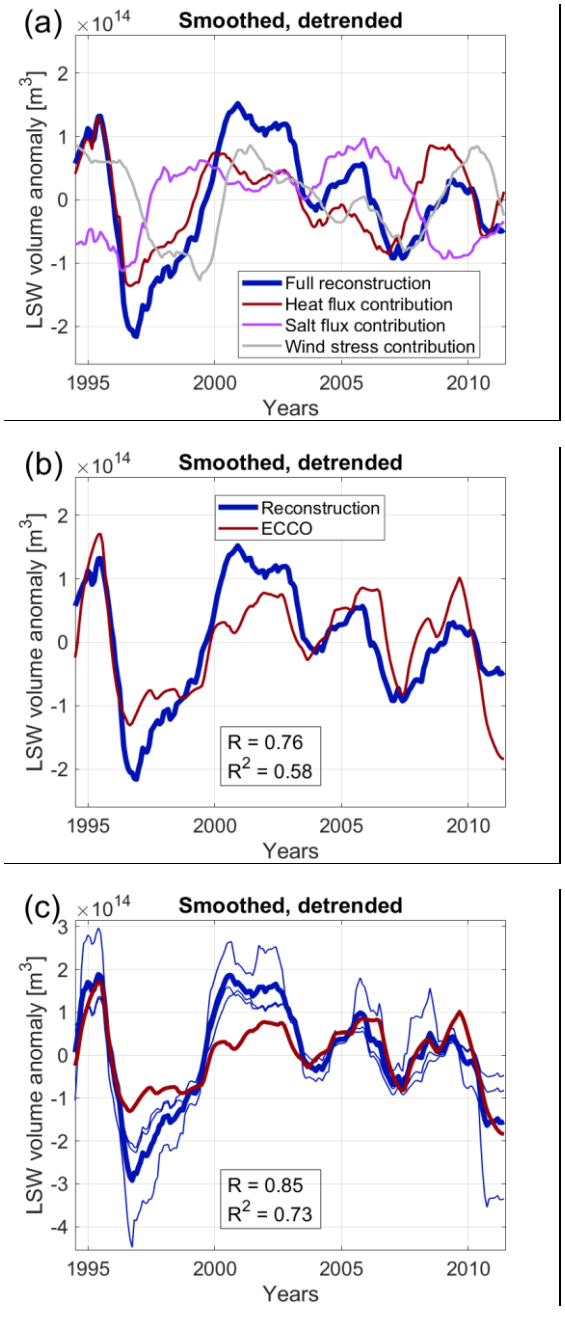

Figure 2: (a) Contribution of wind stress (both zonal and meridional in gray), heat (red), and freshwater fluxes (purple) at the surface to the monthly reconstruction of LSW volume anomalies (blue) relative to the seasonal cycle. The attribution and reconstruction uses sensitivity patterns from objective functions over the spring 2006 – winter 2007 period. The timeseries are smoothed with a 13-month running mean. Each contribution timeseries was detrended. (b) Comparison of the reconstruction (blue) from (a) with the deseasonalized LSW volume anomalies in ECCO (red), smoothed with a 13-month running mean. Detrending was applied after the individual contributions were summed ; (c) Same as (b) but also using winter objective functions in 2006 and 2011 to obtain three different reconstructions (thin blue lines) and a mean estimate (thick blue line). Correlations are shown with respect to the mean reconstruction.

https://doi.org/10.5194/egusphere-2023-1564
Preprint. Discussion started: 13 July 2023

Sea is strictly nonnegative. These deficiencies in the reconstruction are likely due to historical changes in the ocean's background state, as well as processes not captured by the model linearization. Our reconstructions (Fig. 1b) also exhibit mismatches during some of the seasonal transitions from high to low LSW volume. It is also important to point out that we only have ensembles at winter times and not summer or fall when the largest decline of LSW volume occurs. Any small spread between the three reconstructions in the summer and fall is solely due to the subtraction of different time-mean values and the removal of different long-term trends.

We can also compare our result with LSW anomalies relative to the seasonal cycle, where both our reconstruction and the ECCO timeseries are deseasonalized and then smoothed with a 13-month running mean (to mitigate any seasonal bias in our reconstruction). We assume that we need *at least* 24 months of previous history of the surface boundary conditions to reconstruct a given monthly anomaly (Fig. C1). In addition, the 13-month running mean that we apply takes a sliding window of 6 months before and after each reconstructed month. Hence, in our comparison of the deseasonalized smoothed ECCO timeseries and our reconstruction, we leave out the first 24+6 = 30 months of each timeseries. In this case, we are able to recover more than two-thirds of the variability (R=+0.85) in LSW volume (Fig. 2).

Our method allows us to break down the reconstruction into components due to wind-stress, heat flux, and freshwater flux anomalies at the ocean surface. We see comparable contributions from each of these sources of historical variability (Fig. 2). For example, salt fluxes are the main cause behind the 2005 LSW anomaly while both wind stress and heat fluxes contribute in 2007. The 2008 relative increase in LSW explored by Yashayaev and Loder (2009) can be attributed primarily to surface heat fluxes (Fig. 2a). These attribution results hold true across our three reconstructions.

A similar picture emerges when we consider an annually averaged reconstruction of LSW volume anomalies (Fig. 3) relative to the climatological annual mean in ECCO. We once again assume a minimum required time history spanning two years of surface forcing and thus start our comparison in 1994 rather than 1992, the first year of ECCO. In this case, we recover 74% of the ECCO interannual variability (R=+0.86) in LSW volume. Once again, each of the different surface boundary conditions (wind stress, heat, and salt fluxes) make comparable and equally important contributions (Fig. 3).

We then move on to identify geographical regions where the lagged LSW sensitivity to surface boundary conditions is most pronounced at different lead times. At short lead times, the watermass volume is most sensitive to changes in the Labrador Sea itself such as local heat or freshwater flux anomalies (Fig. D1c,d). The sensitivity to zonal winds at short lead times appears spatially noisy (Fig. D1a).

https://doi.org/10.5194/egusphere-2023-1564
Preprint. Discussion started: 13 July 2023

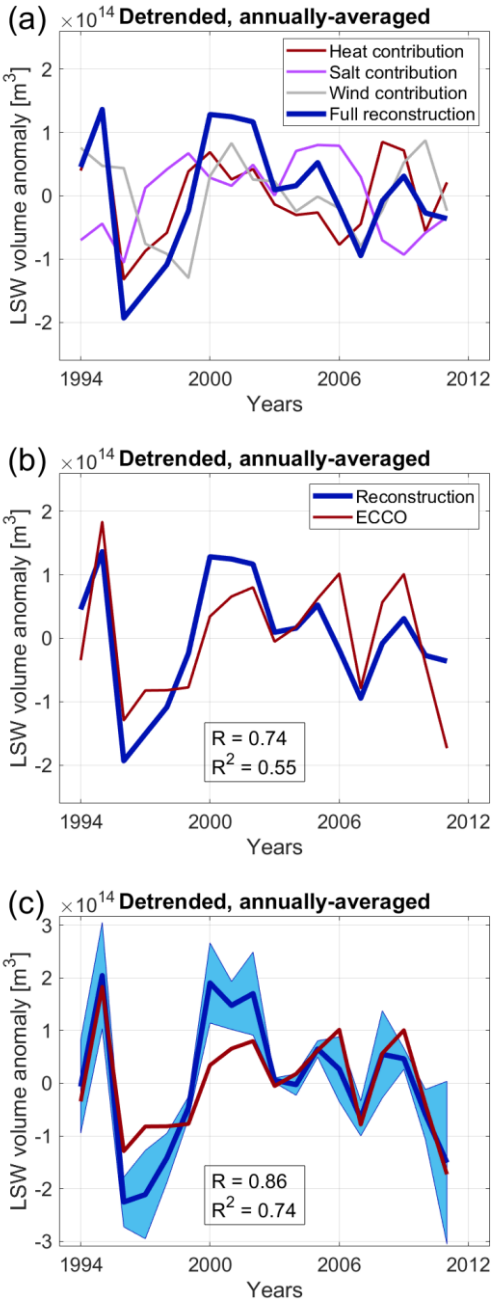

Figure 3: (a) Same as Fig. 2a but for annually-averaged contributions and reconstruction timeseries relative to the annual-mean. (b) and (c) Same as Fig. 2b and Fig. 3c but for annually-averaged anomalies relative to the annual-mean. The shaded envelope in c indicates the difference between the minimum and the maximum of the three reconstructions at each point in time.

At longer lead times of several years, we see sensitivity to wind stress forcing along the West European and Northwest African shelf, especially in the meridional component of wind stress (Fig. 4b,f). Coastal waveguides allow the wind-driven upwelling or downwelling signal to be transmitted to the subpolar gyre, where it alters the SSH and density gradients and

https://doi.org/10.5194/egusphere-2023-1564
Preprint. Discussion started: 13 July 2023

affects geostrophic transport in the North-eastern Atlantic, as suggested by Pillar et al. (2016), Loose et al. (2020), and Kostov et al. (2021).

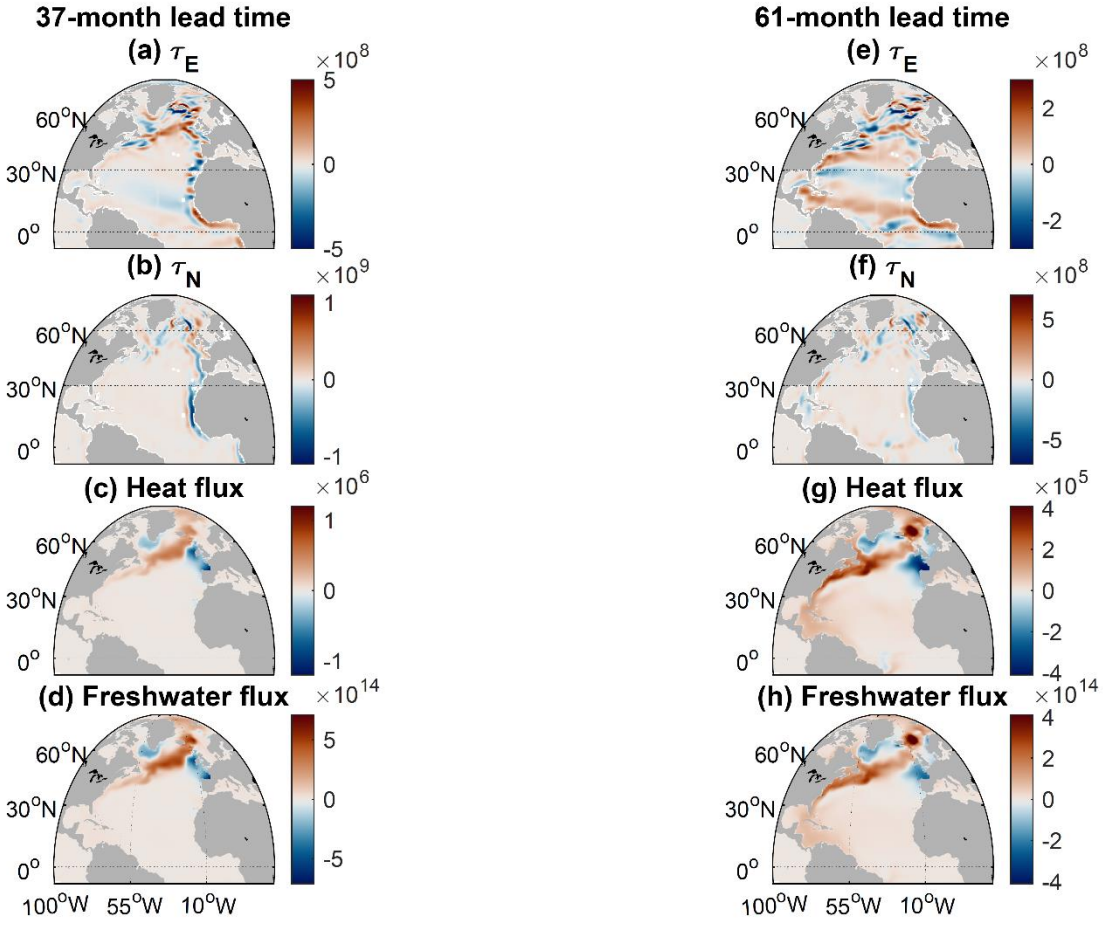

Figure 4: Sensitivity of winter 2007 LSW volume to surface boundary conditions at a lead time of 37 months ((a) through (d)) and 61 months ((e) through (h)). Sensitivity to zonal (a,e) and meridional (b,f) windstress $[m^3N^{-1}m^2]$, surface heat fluxes (c,g) $[m^3W^{-1}m^2]$ out of the ocean, and surface freshwater fluxes $[m^3m^{-1}s]$ out of the ocean (d,h). Red shading indicates that a positive anomaly in the surface boundary condition leads to an increase in LSW volume at the indicated lead time.

At lead times of several years, we also see remote sensitivity to zonal wind stress, but at these lead times the geographical pattern is mostly aligned with the mean pathway of the North Atlantic Current (NAC) branches. This sensitivity along the NAC is well illustrated in Fig. 4a,e and Fig. 5, where we use the climatology of sea surface height (SSH) contours to indicate the location and direction of the time-mean currents in the subpolar gyre, which is largely wind-driven. Hakkinen and Rhines (2009) suggest that the pathways of the NAC branches have exhibited historical shifts affecting the transport of subtropical water to the Nordic Seas between 1991 and 2005. Significant variability in the NAC flow that branches towards

https://doi.org/10.5194/egusphere-2023-1564
Preprint. Discussion started: 13 July 2023

the Nordic Seas has also been observed over the more recent 2008-2016 historical period (Weijer et al. 2022). Raj et al. (2018) and Holliday et al. (2020) suggest that leading modes of atmospheric variability such as the North Atlantic Oscillation can trigger intensification or weakening of the Norwegian Current which branches from the NAC and transports warm water towards the Greenland-Iceland-Norwegian (GIN) Seas.

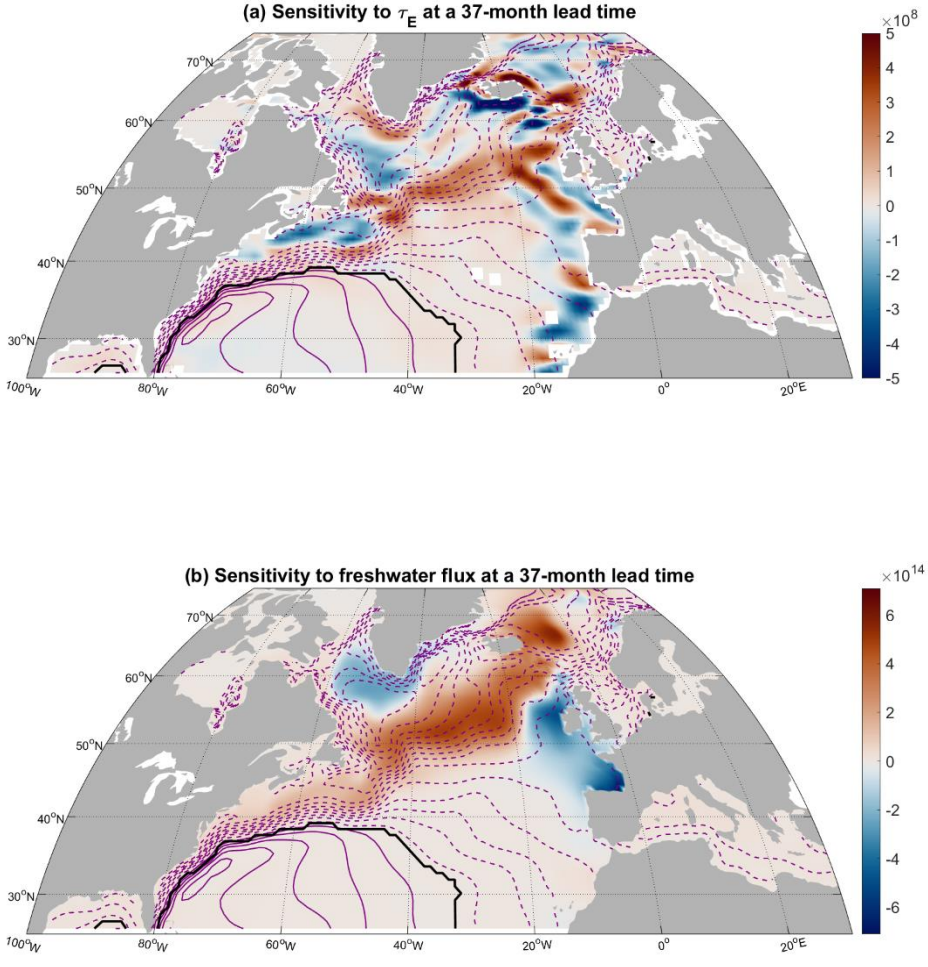

Figure 5: (a) Same as Fig. 4a [$m^3N^{-1}m^2$]; and (b) same as Fig. 4d [$m^3m^{-1}s$], but focusing on the mid and high latitudes. Superimposed are the climatological time-mean SSH contours from the ECCO state estimate, 7 cm apart. Positive contours are solid purple lines, negative contours are dashed, and the zero contour is a thick black line.

At multiannual lead times, we also see sensitivity to surface heat and freshwater fluxes in the GIN Seas themselves (Fig. 4c,g,d,h and Fig. 5), especially in the region of the cyclonic gyre circulation in the Norwegian Basin (Fig 1a and Raj et al., 2019). We also see very pronounced lagged sensitivity of LSW volume to surface heat and freshwater fluxes (Fig. 4c,g,d,h

https://doi.org/10.5194/egusphere-2023-1564
Preprint. Discussion started: 13 July 2023

and Fig. 5) both along the NAC and along its flanks at multiannual lead times (Fig. 4c,g,d,h and Fig. 5). We call these distinctive sensitivity patterns a "Traffic Controller" – we propose that input of momentum or buoyancy with this spatial fingerprint can act to accelerate or decelerate the NAC and deflect it away or towards the Irminger Sea, the Iceland Basin, and the Nordic Seas. This in turn affects the transport of warm, saline subtropical water that subsequently undergoes buoyancy loss in the Iceland and Irminger basins (Petit et al., 2020; Petit et al., 2021) and eventually gets transformed into deeper watermasses such as LSW.

We test our "Traffic Controller" hypothesis in a forward experiment, where we apply the sensitivity pattern from Fig. 4d, rescaled by a factor of (-10^{-22}), as a perturbation of order $10^{-8}\ m\ s^{-1}$ to the background rainfall throughout January 2000 of the ECCO historical state estimate. The period 2000-2008 is marked by a resumption in the formation and storage of relatively larger volumes of LSW (Fig. 1). Hence, launching our experiment in 2000 allows us to explore this regime of enhanced LSW production. We adjust the amplitude of our positive and negative poles in the applied perturbation pattern such that the net input of freshwater is zero. When comparing against the unperturbed ECCO state estimate, we see that indeed, the "Traffic Controller" pattern affects the SSH gradients (Fig. 6a), and hence *decelerates* NAC transport towards the western subpolar gyre and increases northeastward transport towards the Iceland Basin and the GIN Seas. In addition, there is an increase in the southward transport along the East Greenland Shelf (Fig. 6a). Our results also show that surface temperature throughout the subpolar gyre decreases in response to the perturbation, while sea surface salinity exhibits a dipole pattern: freshening along the western boundary of the Labrador Sea and salinification along the Greenland shelf (Fig. 6b,c). Early on in the experiment, the circulation anomaly in the subpolar gyre causes more intense surface heat loss in the Iceland Basin and the Nordic Seas (Fig. 7). This adjustment is followed by more intensive production of LSW water in the Irminger Sea and south of Cape Farewell (Fig. E1a). Some of this water with LSW properties enters the Labrador Sea (Fig. E1b) and increases the volume of stored LSW even in the late summer. Finally, there is enhanced production and storage of LSW in the Labrador Sea itself (Fig. E1c,d). As a result, the volume of accumulated LSW in the Labrador Sea increases (Fig. E2). Using Eq. (7) and surface boundary conditions from the surface freshwater flux experiment, we are largely able to recover the evolution of the LSW volume anomaly in the basin (Fig. E2). This serves as additional independent verification of our reconstruction methodology. Both the experimental output and our reconstruction show that the "Traffic Controller" pattern of surface freshwater fluxes impacts LSW on a timescale of several years.

https://doi.org/10.5194/egusphere-2023-1564
Preprint. Discussion started: 13 July 2023

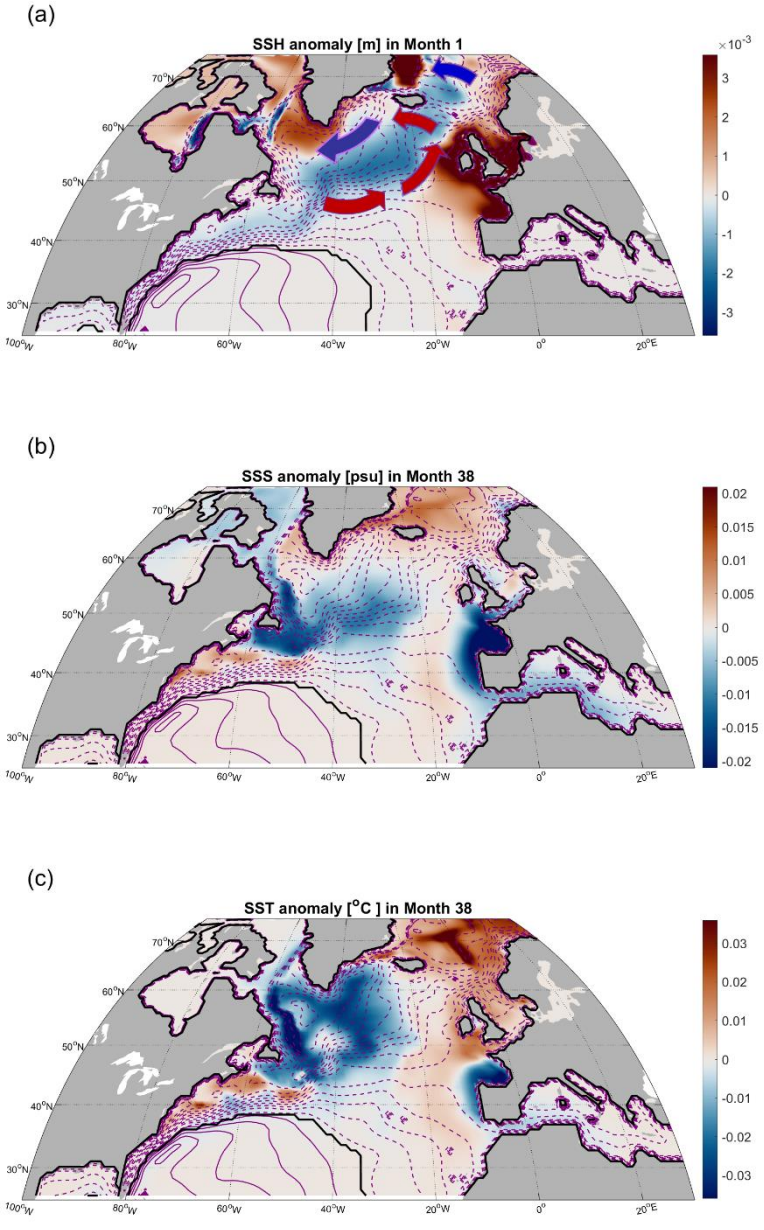

Figure 6: (a) Monthly-mean SSH anomaly ([cm] shaded, positive in red, negative in blue) from Month 1 of the freshwater perturbation experiment relative to the unperturbed ECCO state estimate. Superimposed are the corresponding SSH contours from the unperturbed ECCO state estimate, 7 cm apart. Positive contours are solid purple lines, negative contours are dashed, and the zero contour is a thick black line. Schematic arrows indicate the impact of the SSH anomalies on the anomalous circulation pattern: increased northeastward transport towards the Iceland basin and increased southward transport along the East Greenland Shelf; (b) Same as in a but shading indicates the contemporaneous SSS anomaly [psu] in Month 38 of the freshwater perturbation experiment and the corresponding SSH contours from the unperturbed ECCO state estimate. (c) Same as in b but shading indicates the SST anomaly [°C].

https://doi.org/10.5194/egusphere-2023-1564
Preprint. Discussion started: 13 July 2023

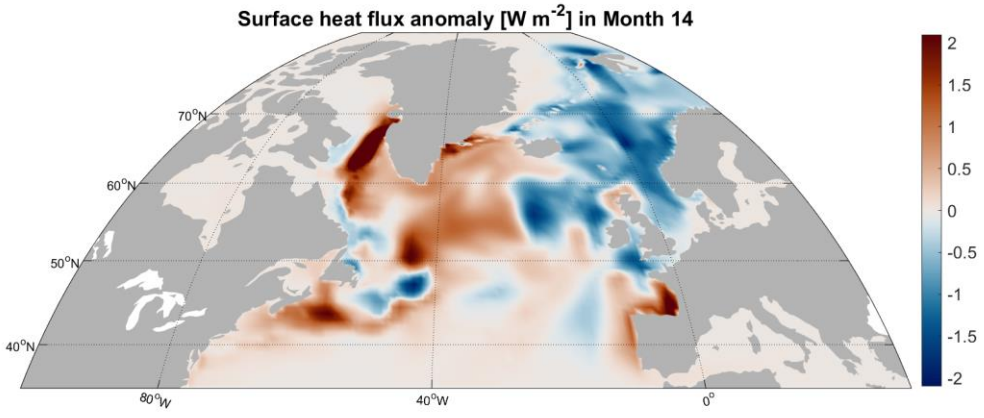

Figure 7: Monthly-averaged surface heat flux anomaly [$W\ m^{-2}$] 14 months after the surface freshwater perturbation applied in January 2000 of the ECCO state estimate. Blue shading indicates anomalous surface heat loss from the ocean to the atmosphere, and red shading corresponds to anomalous uptake of heat into the ocean.

However, the "Traffic Controller" pattern is an abstract construct: a sensitivity to hypothetical surface forcing anomalies at each model grid point. To assess whether this genuinely gives rise to LSW volume variability, we also need to know whether there is actual historical variability in the ECCO surface boundary conditions that projects on this sensitivity pattern and activates it. To that end, we consider the standard deviation of surface heat and freshwater fluxes at each grid point to obtain a map of surface variability for each month of the year relative to the seasonal cycle (Fig. 8). As expected for a high latitude region, the variability is larger in the winter season (not shown). The pattern of surface flux variability is also intensified near the western boundaries of the basins. In particular, the winter-time surface freshwater fluxes exhibit some of the strongest variability along the western boundary of the Labrador Sea (Fig. 8b) in the marginal sea-ice zone (Petit et al., 2022, submitted). We project the wintertime surface flux variability patterns onto the corresponding "Traffic Controller" sensitivity patterns to see where heat and salt fluxes contribute the most to the delayed response of LSW volume with a lag of 5 years (Fig. 9). Once again, the western boundaries of the North Atlantic and its marginal seas appear to be a prominent source of LSW variability at a lead time of 5 years (Fig. 9b).

https://doi.org/10.5194/egusphere-2023-1564
Preprint. Discussion started: 13 July 2023

370

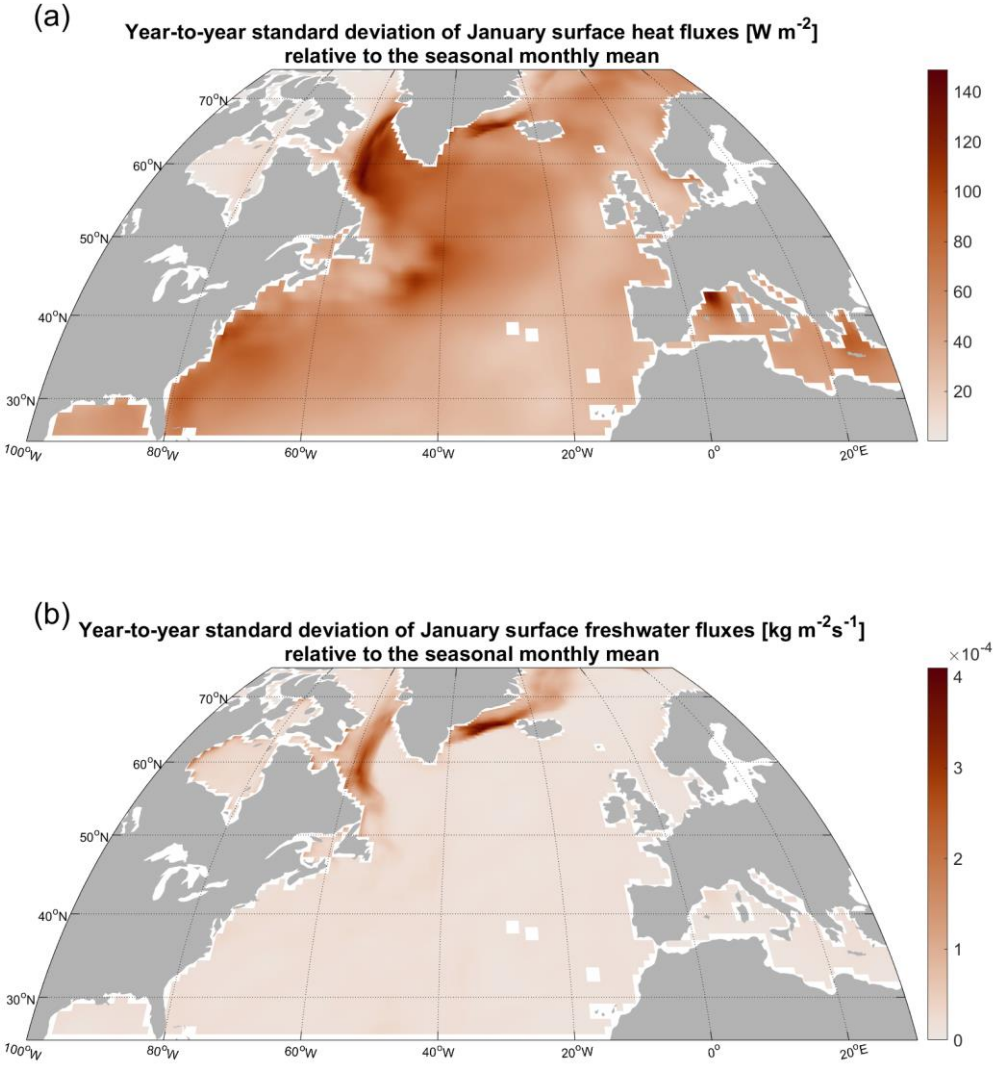

375 **Figure 8: (a) Year-to-year standard deviation of the January surface heat fluxes [Wm^{-2}] at each model grid point in the ECCO state estimate ; (b) same as in a but for surface freshwater fluxes [$m\ s^{-1}$]**

https://doi.org/10.5194/egusphere-2023-1564
Preprint. Discussion started: 13 July 2023

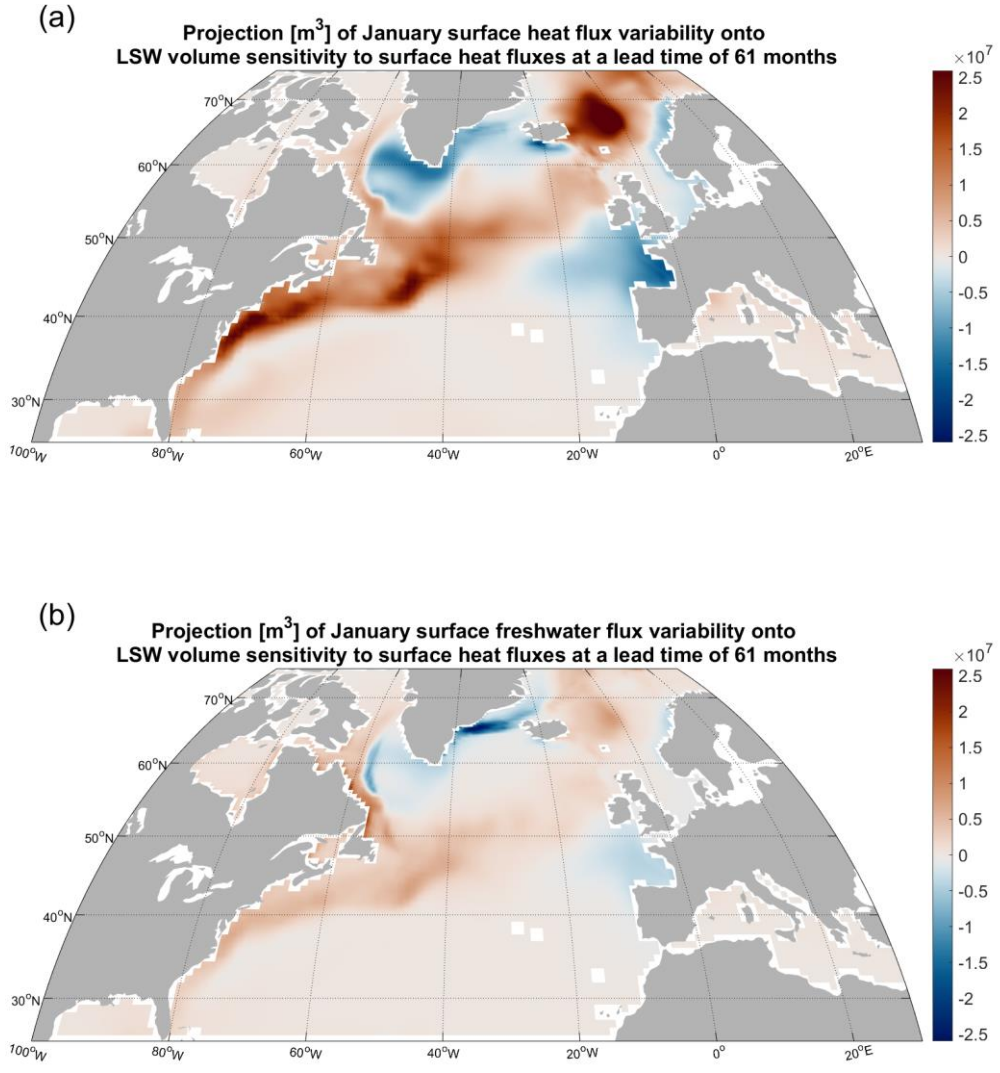

380

Figure 9: (a) Projection [m^3] of the surface heat flux variability from Fig. 8a onto the sensitivity of LSW to surface heat fluxes at a lead time of 5 years from Fig. 4g. (b) Projection [m^3] of the surface freshwater flux variability from Fig. 8b onto the sensitivity of LSW to surface freshwater fluxes at a lead time of 5 years from Fig. 4h.

We also explore if there are preferred lead-lag relationships in the system by looking at weighted lagged correlations
385 (Eq. (11)). As expected, we find that the contributions of surface heat and freshwater fluxes over the Labrador Sea interior (bottom depth larger than 2.5 km), over the Southeast Greenland Shelf, and over the Western Irminger Sea exhibit short characteristic lead times (Fig. 10a,b and Fig. F2a,b). In comparison, surface fluxes of heat, freshwater, and momentum along the NAC pathway drive LSW volume anomalies both at short lead times but also with a lag greater than 2 years (Fig. 10c and

https://doi.org/10.5194/egusphere-2023-1564
Preprint. Discussion started: 13 July 2023

Fig. F2c). The large magnitude of LSW volume variability generated by boundary conditions along the NAC further highlights the importance of this advective pathway, especially at interannual lead times (Fig. 10c and Fig. F2c). Surface buoyancy fluxes along Labrador Sea Western Boundary (sea floor shallower than 2 km) drive even more delayed responses, peaking at lead times greater than 4 years (Fig. 10d and Fig. F2d), consistent with the findings of Kostov et al. (2022).

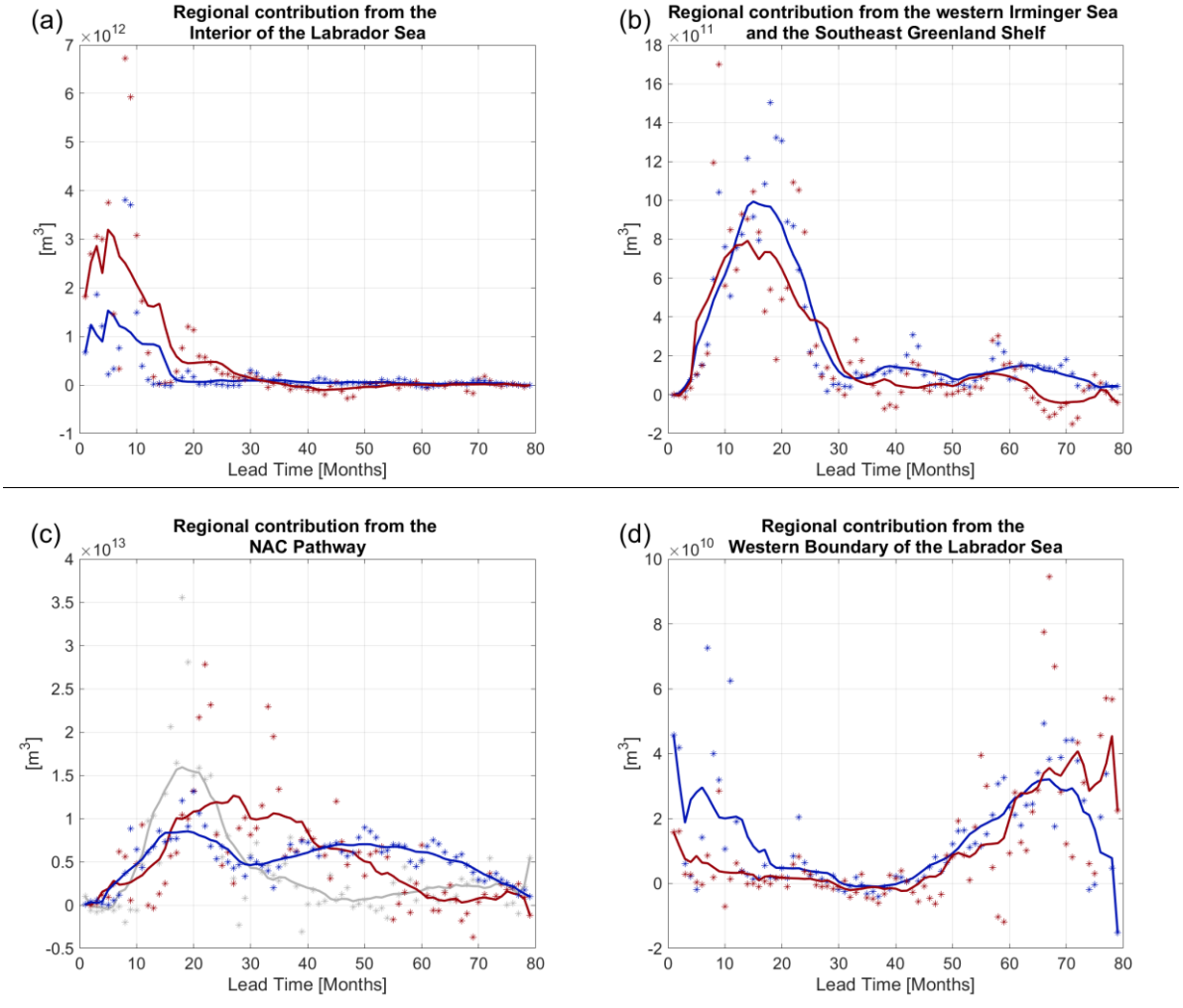

Figure 10: Preferred lead times in the regional contributions of surface boundary conditions to LSW variability $[m^3]$, Eq. (11) over (a) the Labrador Sea interior (the region with bottom depth larger than 2.5 km, as shown in Fig. F1a); (b) the western part of the Irminger Sea and the southeast Greenland shelf (region shown in Fig. F1b); (c) the NAC pathway over the region defined in Appendix F and Fig. F1c; and (d) Labrador Sea Western Boundary, defined as the area shallower than 2 km and south of 59°N (as in Fig. F1d). The horizontal axis denotes the lead time. Shown are the regional contributions of surface heat fluxes (red), freshwater fluxes (blue), and zonal wind stress (gray, panel b only) to intermonthly variability in LSW volume. Asterisks correspond to monthly data points, while the solid lines represent running means averaging the data points over 13-month windows. Only sensitivity patterns from spring 2006 – winter 2007 objective functions are used in the calculation.

https://doi.org/10.5194/egusphere-2023-1564
Preprint. Discussion started: 13 July 2023

The existence of such long characteristic lead times in the system suggests some degree of predictability of LSW variability into the future. We explore the predictability of annually-averaged LSW volume anomalies at a time horizon of 1 year by applying the modified convolution from Eq. (8). We thus omit information about the surface boundary conditions at zero lag, and when reconstructing LSW anomalies in each year, we only include past information from the preceding years. We show that using historical information alone, we can predict 41% of LSW volume variability (R=0.64) a year into the future (Fig. 11), when we use the sensitivity patterns of our 2006-2007 objective functions. This skill is not sufficient for making reliable long-range predictions of watermass anomalies but demonstrates the propensity of LSW for a delayed response to surface forcing away from the interior of the Labrador Sea. Our skill decreases drastically if we extend our annual-mean prediction two years into the future (not shown). This sharp decline in prediction skill is not a surprise, as the responses to surface heat and momentum fluxes along the NAC exhibit peaks at lead times of roughly 1.5 to 2.5 years (Fig. 10c and F2c).

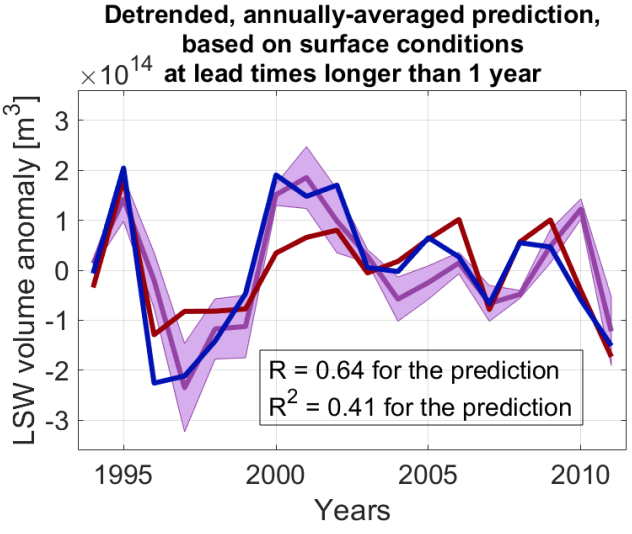

Figure 11: Annually-averaged prediction (dark purple) of LSW volume anomalies relative to the annual mean at a time horizon of 1 year into the future. The shaded envelope reflects the uncertainty of the prediction estimated analogously to the uncertainty in Fig. 3c. Superimposed is the full reconstruction from Fig. 3c (blue) that also includes information about surface boundary conditions at zero lag. The actual ECCO anomalies in LSW volume relative to the annual cycle are shown in red. The reconstruction skill (R=+0.64) for a prediction one year into the future, shown here, is much larger than the reconstruction skill for a prediction two years into the future (not shown).

4. Discussion and Conclusion

In this study, we have presented a novel linear reconstruction of accumulated LSW volume in the Labrador Sea using *only* surface boundary conditions: wind-stress and surface heat and freshwater fluxes. In addition, we offer a *causal* attribution of historical LSW variability. Our results suggest that wind stress, freshwater fluxes, and heat fluxes make contributions of comparable magnitude to LSW volume anomalies (Fig. 2 and Fig. 3). This challenges the traditional view that wintertime cooling in the Labrador Sea is the dominant driver of variability in the volume of North Atlantic Deepwater (NADW) masses.

https://doi.org/10.5194/egusphere-2023-1564
Preprint. Discussion started: 13 July 2023

We furthermore show that surface boundary condition anomalies away from the Labrador Sea can trigger significant delayed responses of LSW. For example, the watermass volume is sensitive to meridional wind stress along the eastern boundary of the North Atlantic, all the way to Western Africa. A wave signal from this region is quickly communicated along the coastal waveguide to the subpolar gyre (Pillar et al. (2016); Kostov et al., 2021; Loose et al., 2020). Our findings are thus similar to the results of Jones et al. (2018), who highlight similar enhanced sensitivity of total heat content in the Labrador Sea to wind stress along the African and West European shelves.

Our results also indicate that the LSW volume is particularly sensitive to remote zonal wind and buoyancy forcing along the pathway of the NAC but also on its flanks, extending westwards towards the Labrador Sea and eastwards towards the European Basin. We refer to the geographical fingerprint of this remote sensitivity as the "Traffic Controller" pattern: in effect, SSH and surface density anomalies aligned with the NAC branches can accelerate or decelerate the currents and divert them away or towards the Irminger Sea, the Iceland Basin, the Nordic Seas. Similarly, the input of momentum by surface winds also impacts the NAC branches. This modulates the transport of warm, saline subtropical water that loses buoyancy in the Iceland Basin and the Irminger Sea (Petit et al., 2020; Petit et al., 2021) and is subsequently be transformed into LSW.

The "Traffic Controller" sensitivity pattern appears to be activated on a regular basis by large SSS variability originating along the Western Boundary of the Labrador Sea. The same region has also been shown to be an important driver of subtropical AMOC variability (Kostov et al., 2021; Kostov et al., 2022). The Labrador Sea Western Boundary is a marginal sea ice zone, where changes in freezing, melting, and the ice distribution strongly affect the salinity budget of the upper ocean. The model representation of these ice-driven SSS fluctuations is sensitive to the resolution of the ocean domain and may be a significant source of bias in historical simulations (Petit et al., 2022, submitted).

We show that the contribution of SSS variability in the Labrador Sea marginal sea ice zone to LSW volume anomalies is a delayed response with a preferred lead-time of more than 3 years. This is consistent with the experiments in Kostov et al. (2022) who suggest that freshening along the western boundary of the basin impacts LSW with a lag of five years.

Notably, surface momentum and buoyancy fluxes along the NAC pathway also trigger anomalies in LSW volume with lags on a timescale of 2 to 5 years. The existence of such large delayed responses in the ocean system implies a certain degree of predictability of LSW anomalies and suggests that the NAC is one of the major sources of predictive skill.

We have tested the predictability of LSW anomalies a year into the future using only past information about surface boundary conditions. We demonstrate that we can estimate approximately 41% of LSW variability at a time horizon of 1 year into the future. This substantial predictive skill at a 1-year horizon suggests that local conditions in the Labrador Sea at zero lead time are not the only important driver of LSW volume anomalies. Our results imply that preconditioning in the North Atlantic away from the Labrador Sea plays a key role in driving watermass variability. In particular, our results suggest that anomalies in the NAC transport of heat and salt modulate surface-forced watermass transformation in the eastern subpolar gyre (and the GIN Seas), which then affects the production of LSW downstream in the Irminger and Labrador Seas. This agrees with the findings of Petit et al. (2021) who show that air-sea fluxes in the eastern subpolar gyre dominate the variability of low-stratified mode water that acts as a precursor to the formation of LSW. We therefore suggest that our reconstructions

https://doi.org/10.5194/egusphere-2023-1564
Preprint. Discussion started: 13 July 2023

and predictions should not be judged merely on the basis of their skill. Our analysis sheds light on the importance of various physical processes that affect the accumulation of LSW in the Labrador Sea.

The scope of our study is limited by the methods we use. We rely on linear response theory which may not hold in the case of regime shifts in the North Atlantic circulation. More generally, we do not account for nonlinearity in the LSW response. In addition, we compute our objective function, watermass volume, only over particular historical periods, spring 2006-early 2007, as well as March 2006 and March 2011. We expect that linearizing the model about an earlier or later period may produce different sensitivities of LSW to surface boundary conditions. For example, the LSW formation sites and export pathways may change in time. This impact of the background ocean state on the sensitivity of LSW is reflected in the envelope of uncertainty on our reconstructions. Similarly, including a longer time history of past surface forcing can affect our results. Other limitations come from the fact that we use a general circulation model to estimate the sensitivity of LSW to boundary conditions. Our lagged sensitivity patterns inevitably depend on the model dynamics and any bias therein. For example, the model configuration in this study does not resolve eddies, which can significantly impact ocean transport and variability in the subpolar gyre (e.g., Zhao et al., 2018).

Such potential sources of model bias are mitigated by the fact that we use the ECCO configuration of the MITgcm, a state-estimate which is constrained by available historical observations in a least squared sense (Forget et al, 2015). This gives us confidence that our analysis is relevant to real-world ocean dynamics and gives an insight into processes affecting the volume budget of the important LSW watermass. In this study we focus on the watermass volume budget, but the same approach can be extended to a future analysis of LSW heat content variability.

Appendix A. Activation Functions

In our definition of LSW volume as a numerical objective function (Eq. (5)), we employ logistic activation functions to approximate Boolean conditions. For example, the condition that LSW potential density $\sigma_\theta > \sigma_{\theta\ lower} = 27.7\text{kg m}^{-3}$ (Eq. (1)) is expressed as

$$(1/2 + \tanh((\sigma_\theta - \sigma_{\theta\ lower})\, c)/2),\ c = 10^5\ kg^{-1}\ m^3 \quad \text{(A1)}$$

The above expression asymptotes to zero as σ_θ decreases below the lower bound $\sigma_{\theta\ lower} = 27.7\text{kg m}^{-3}$ and asymptotes to 1 as σ_θ increases above $\sigma_{\theta\ lower}$ (see Fig. A1a for an illustrative example of an activation function). Because the constant factor $c = 10^5\ kg^{-1}\ m^3$ is very large, the activation function (Eq. (A1)) has a very steep slope near $\sigma_{\theta\ lower}$. An offline calculation shows that the activation functions in Eq. (5) give the same result for the volume of LSW in the Labrador Sea in ECCO as the Boolean conditions (Eq. (1) and (2)) within numerical precision.

The derivative of our activation functions with respect to the input is approximately zero everywhere except in a range of input values close to the imposed upper and lower bounds that define LSW:

$$\sigma_{\theta\ lower} = 27.7\text{kg m}^{-3},\ \sigma_{\theta\ upper} = 27.84\text{kg m}^{-3},\ \text{PV}_{\text{upper}} = 4 \times 10^{-12}\ m^{-1}s^{-1}$$

https://doi.org/10.5194/egusphere-2023-1564
Preprint. Discussion started: 13 July 2023

(see for example the shaded area in Fig. A1). Therefore, our objective function, as defined in Eq. (5) has nonzero derivatives only when a model grid cell in the Labrador Sea reaches σ_θ or PV values near these thresholds. In these transitional ranges, the activation functions have a maximum slope of $c/2$, equal to $5 \times 10^4\ kg^{-1}\ m^3$ or $5 \times 10^4\ m\ s$ in our case.

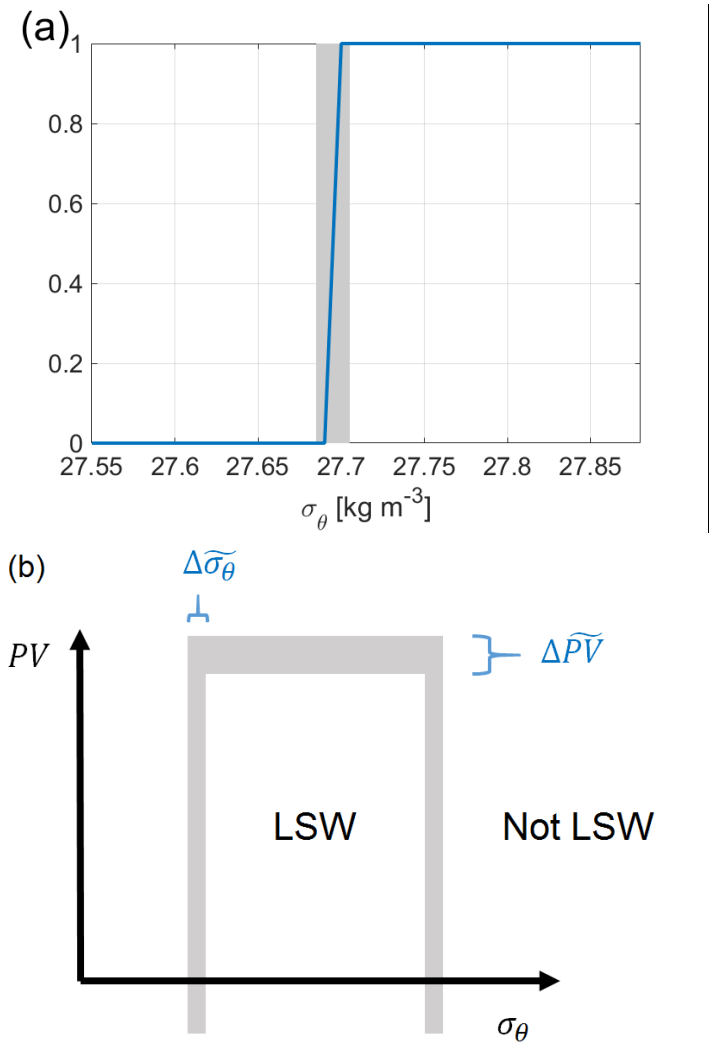

Figure A1: (a) An illustrative example of a logistic activation function that imposes the condition $\sigma_\theta > \sigma_{\theta\ lower} = 27.7\ kg\ m^{-3}$. Gray shading indicates a transition region where the value of the activation function is between 0 and 1. Over this region, the average slope of the activation function is ≈1/(width of the shaded area) in units of $kg^{-1}\ m^3$; (b) a schematic of the definition of LSW in potential density and PV space with the transition regions illustrated in a shown with gray shading. The activation functions have a slope close to 0 outside the transition regions.

This raises the question whether the chosen large values of $c = 10^5\ kg^{-1}\ m^3$ and $c = 10^5\ m\ s$ affect the derivatives of the objective function. Have we arbitrarily rescaled the sensitivity patterns by factor c? In this context, an important point to consider is that in our adjoint calculations, the objective function is not evaluated during a single model timestep of 1 hour,

https://doi.org/10.5194/egusphere-2023-1564
Preprint. Discussion started: 13 July 2023

but is averaged over a time period corresponding to 1 simulated month. Hence, Labrador Sea grid cells that enter or leave the LSW potential density and potential vorticity range spend many model timesteps gradually evolving across the transitional regime near the $\sigma_{\theta\ lower}$, $\sigma_{\theta\ upper}$, and/or PV_{upper} thresholds (for example, the shaded region in Fig. A1). In addition, the objective function is defined over a large spatial region, the entire Labrador Sea. When a model grid cell in the region of interest enters or leaves the LSW potential density or potential vorticity range, this transition involves adjacent grid cells, too. The objective function that we define averages temporally over 1 month and spatially over each group of grid cells that transition from one watermass to another.

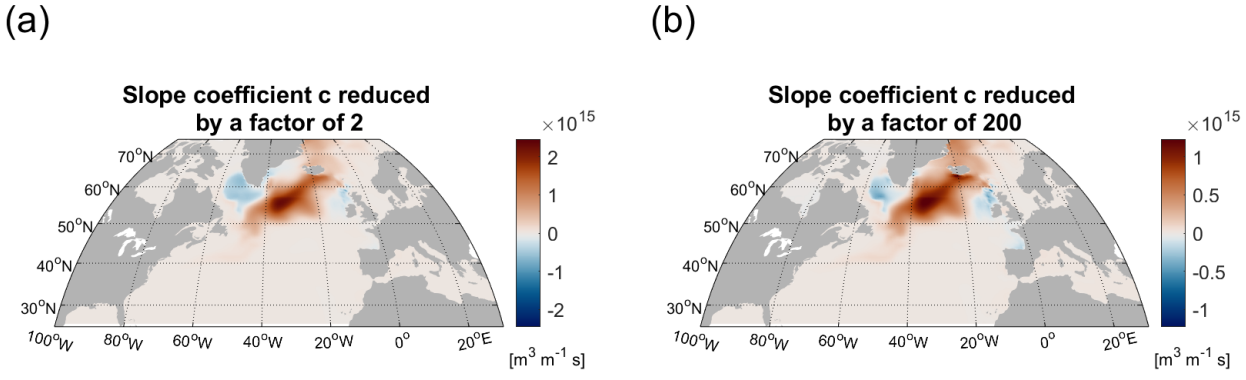

Figure A2: (a) Sensitivity of the LSW volume to surface freshwater flux anomalies $[m^3 m^{-1} s]$ at a lead time of 2 years, where the objective function is defined using the default activation functions with $c = 5 \times 10^4\ kg^{-1}\ m^3$ for potential density and with $c = 5 \times 10^4\ m\ s$ for potential vorticity, respectively. (b) same as in a but with activation function parameters set to $c = 5 \times 10^2\ kg^{-1}\ m^3$ for potential density and with $c = 5 \times 10^2\ m\ s$ for potential vorticity. The limits of the colorbar in a are exactly twice as large as the colorbar limits in b.

Modifying factor c changes only the weight that we assign to a grid cell undergoing transformation relative to its neighboring grid cells and the weight of some days of the month in which we average the objective function relative to other days of the same month. However, the average weight of all transitioning cells remains the same even if we change factor c. Given enough temporal and spatial data points throughout the transition region (e.g., shaded area in Fig. A1), the slope of the applied activation function always averages to 1/(the width of a transitional range) across the transitional regime between LSW and non-LSW water. That is because the logistic activation function always increases from ≈ 0 to ≈ 1 in the transition range, as shown in Fig. A1 (shaded area). This result holds irrespective of the value of parameter c and the maximum slope $c/2$, so long as the slope of the activation function is close to zero outside the transition range (Fig. A1, shaded area). Thus, we do not expect that in the case of our monthly-averaged basin-wide objective functions, the order of magnitude of c will affect the order of magnitude of the sensitivity patterns.

We test this assumption by conducting a set of adjoint calculations with a value of c varied by different orders of magnitude between $c = 5 \times 10^4\ kg^{-1}\ m^3$ and $c = 5 \times 10^4\ m\ s$ on one hand, and $c = 5 \times 10^2\ kg^{-1}\ m^3$ and $c = 5 \times 10^2$

https://doi.org/10.5194/egusphere-2023-1564
Preprint. Discussion started: 13 July 2023

$m\ s$ on the other hand. We otherwise keep all model settings the same. We compare the results for the lagged sensitivity of LSW volume to surface freshwater flux with the new results with reduced c (Fig. A2). We see that over a range of lead times, the sensitivity patterns with different choices of c remain almost identical in their magnitude and geographical fingerprint. The difference between the corresponding patterns is much smaller – roughly a factor of two – which is orders of magnitude smaller than the factor of 100 by which we vary c (Fig. A2). This dependence on the choice of factor c is also smaller than the change in the adjoint sensitivity patterns and adjoint-based reconstructions that we see when we linearize over different time periods from the ECCO historical simulation (e.g., the different individual reconstructions in Fig. 2c). This gives us confidence that the arbitrary choice of c does not affect the validity of our results regarding the volume of LSW, but at the same time we caution that our approach is not universally valid for any objective function of interest. In other words, there are ocean indices for which our method may not be applicable. In our case, changing the value of c, may reduce or increase the skill of our reconstruction, but we have not explored the possibility of tuning this parameter. Instead, we have focused on explaining the physical mechanisms revealed by our analysis.

Appendix B. Atmospheric and oceanic regimes in the ECCO state estimate

To compute the lagged sensitivity of LSW volume to surface boundary conditions, we linearize the model trajectory about particular background states of the system. When we compute winter LSW volume as our objective function, we consider the years 2006, 2007, and 2011. These years represent three different states of the North Atlantic Oscillation (NAO, Fig. B1) based on the National Oceanic and Atmospheric Administration (NOAA) NAO index (https://www.cpc.ncep.noaa.gov/products/precip/CWlink/pna/nao.shtml). The NAO is an atmospheric regime that influences subpolar variability (Roussenov et al., 2022). Similarly, these three years correspond to different winter mixed layer depths in the Labrador Sea and different volumes of LSW. Within our small ensemble, the skill of our linear reconstructions seems to be strongly related to the background LSW volume in the year when we compute the objective function. The timeseries showing the most extreme fluctuations in Fig. 2c corresponds to a reconstruction that uses the sensitivity of winter 2006 LSW volume to past surface boundary conditions.

https://doi.org/10.5194/egusphere-2023-1564
Preprint. Discussion started: 13 July 2023

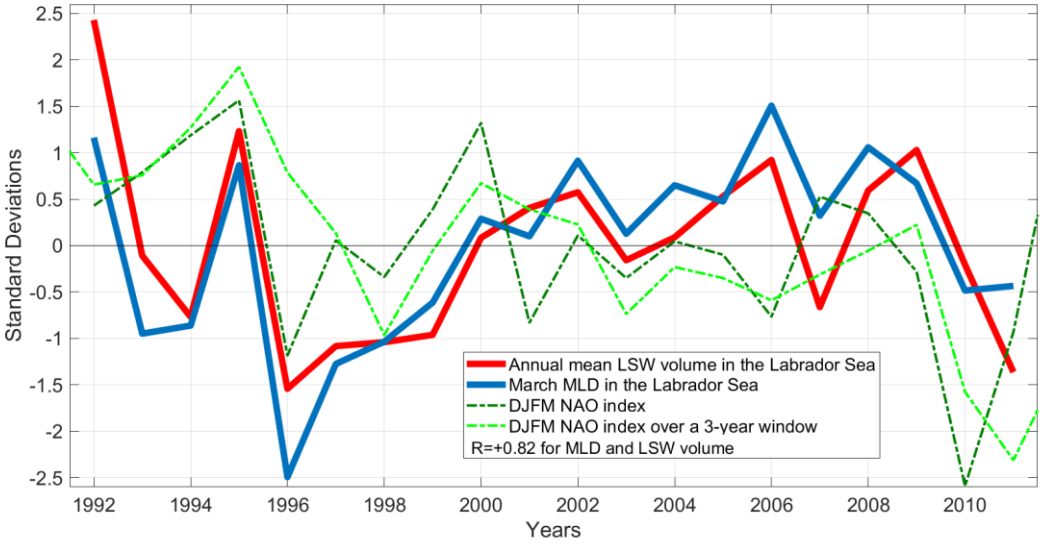

Figure B1: Annual mean LSW volume in the Labrador Sea (red) in ECCO ; March mixed layer depth in the Labrador Sea (blue) in ECCO; December-January-February-March NAO index (dark green) from the NOAA database (https://www.cpc.ncep.noaa.gov/products/precip/CWlink/pna/nao.shtml). A positive NAO phase is associated with lower sea level pressure above Iceland; December-January-February-March NAO index from the NOAA database (dark green) averaged over each year and the preceding 2 years (light green). All indices were normalized by the standard deviation, and the time-mean was subtracted.

Our small ensemble size does not allow us to comment on the ability of the NAO to influence our reconstruction skill. However, we see a strong correlation between winter NAO variability and variability in the Labrador Sea March mixed layer depth and annual-mean LSW volume anomalies (Fig. B1).

Appendix C. Assumed memory of past surface boundary conditions

In our reconstructions, we have to assume a cut-off lead time t_{cutoff} on a timescale of years even though the ocean retains memory of past surface boundary conditions on much longer timescales. We are limited by computational resources and by

https://doi.org/10.5194/egusphere-2023-1564
Preprint. Discussion started: 13 July 2023

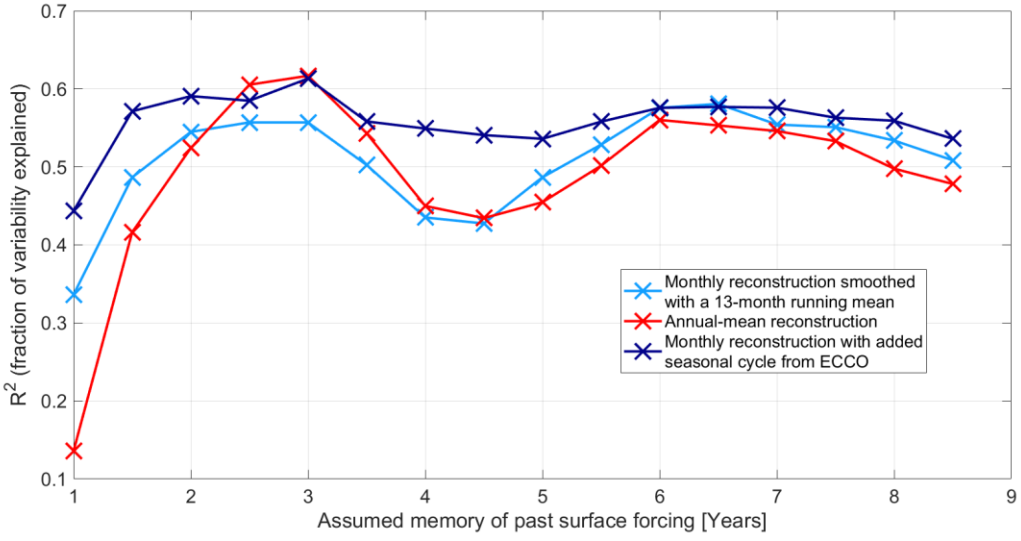

Figure C1: Sensitivity of the reconstruction skill with respect to the assumed memory of past surface forcing (cut-off lead time t_{cutoff}). The reconstructions here use only adjoint sensitivities from objective functions representing LSW volume over the spring 2006 – winter 2007 time period. Light blue crosses show the skill of monthly reconstructions smoothed with a 13-month running mean that recover anomalies relative to the seasonal cycle. Red crosses correspond to annual-mean reconstructions relative to the long-term mean. Dark blue crosses show the skill of monthly reconstructions superimposed on the time-mean seasonal cycle from ECCO, compared against the monthly timeseries from ECCO.

the fact that the ECCO run, which we linearize about, starts in 1992. Last but not least, the adjoint linearization at high latitudes may become less reliable on long timescales.

We test how our reconstruction skill changes as we vary the cut-off lead time t_{cutoff} (Fig. C1). We find that both the monthly and annual-mean reconstructions improve noticeably if we take into account surface boundary conditions going more than 2.5 years back in time. The reconstruction skill declines if we assume a memory of surface conditions longer than 6.5 years (Fig. C1). We thus set the cut-off lead time $t_{cutoff} = 6.5$ years for all points on the timeseries where data for the preceding 6.5 years is available from ECCO.

Appendix D. Sensitivity of LSW to boundary conditions at short lead times

At short lead times, LSW volume is particularly sensitive to local surface buoyancy anomalies in the Labrador Sea (Fig. D1c,d). The sensitivity to zonal winds is also most pronounced in the Labraror Sea itself (Fig. D1a), but is marked by spatial noise.

https://doi.org/10.5194/egusphere-2023-1564
Preprint. Discussion started: 13 July 2023

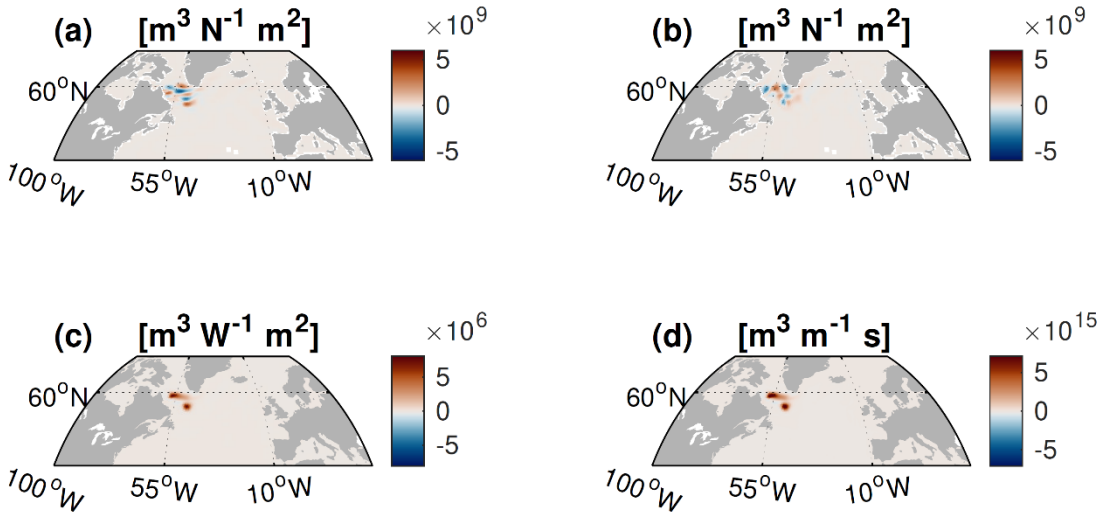

Figure D1: Sensitivity of winter 2007 LSW volume to surface boundary conditions at a lead time of 1 month. Sensitivity to zonal (a) and meridional (b) windstress [$m^3N^{-1}m^2$], surface heat fluxes (c) [$m^3W^{-1}m^2$] out of the ocean, and surface freshwater fluxes [$m^3m^{-1}s$] out of the ocean (d). Red shading indicates that a positive anomaly in the surface boundary condition leads to an increase in LSW volume at a lead time of 1 month.

Appendix E. Adjustment of the North Atlantic Subpolar Gyre in response to the imposed surface freshening and salinification perturbation

We explore in greater detail the ocean's response to the freshening and salinification perturbation applied in January 2000 of the ECCO state estimate and discussed in Section 3. The adjustment of the subpolar gyre gives rise to a dipole in surface heat fluxes with anomalous cooling over the Iceland Basin a year into the experiment (Fig. 7). This preconditions enhanced LSW formation. We first see an increase in LSW production in the Irminger Sea (Fig. E1a), then a thickening of the LSW layer near Cape Farewell (Fig. E1b), and finally, a thickening of the LSW layer across the Labrador Sea (Fig. E1c,d). After a transient decline in LSW volume, these processes eventually give rise to an overall increase in the volume of LSW stored in the Labrador Sea on a timescale of several years after the perturbation (Fig. E2). Notice that the LSW volume anomaly in the Labrador Sea (Fig. E2) reaches a peak during summer months, 2.5 years after the applied perturbation, and some of the LSW thickening in the Labrador Sea is very pronounced near the southeast Greenland Shelf (Fig. E1b). This is consistent with the explanation that a fraction of the additional LSW is not produced locally in the Labrador Sea but is imported as an anomaly from the Iminger Basin following an advective pathway around southern Greenland. At the same time, there are indications that there is a reduction in the southward and eastward export of LSW (blue shading in Fig. E1c) relative to the unperturbed state. Furthermore, the cold anomaly in the Labrador Sea (Fig. 6c) likely acts to decrease the rate of seasonal restratification of LSW.

https://doi.org/10.5194/egusphere-2023-1564
Preprint. Discussion started: 13 July 2023

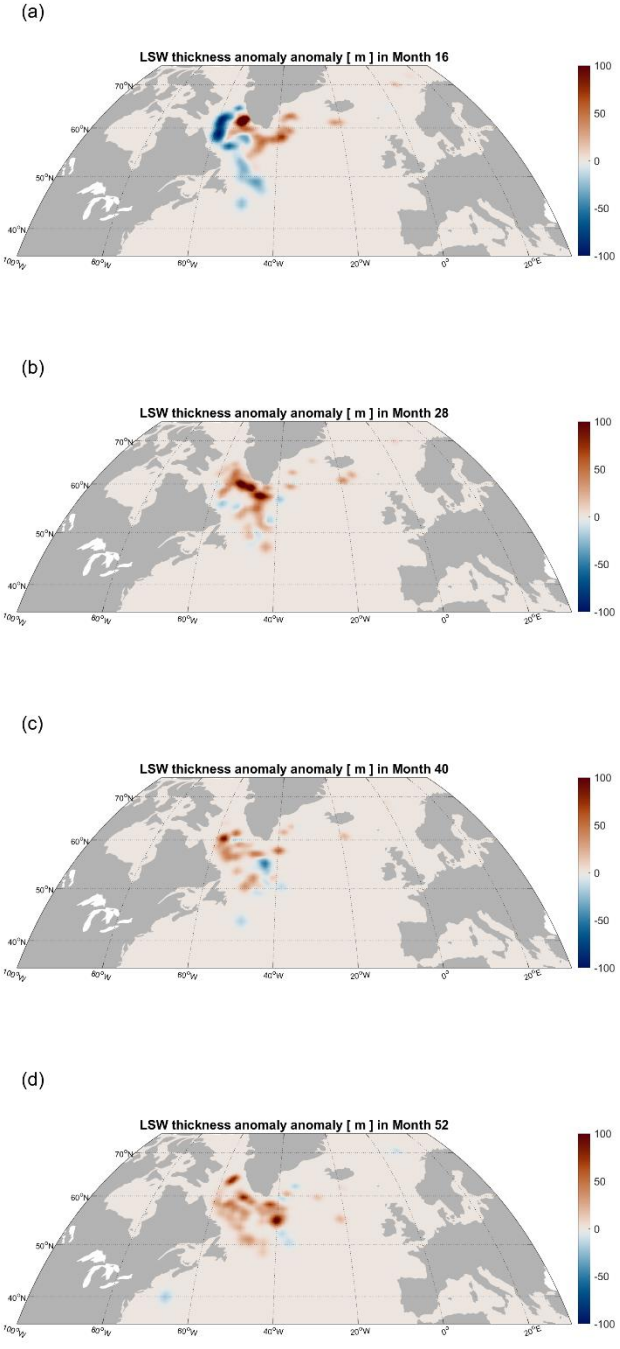

610

Figure E1: Time-evolving anomaly in the thickness [m] of the LSW layer in response to the freshwater flux perturbation pattern applied in January 2000 of the ECCO state estimate. The panels correspond to monthly averages at (a) 16 ; (b) 28 ; (c) 40 ; and (d) 52 months after the freshwater flux perturbation.

https://doi.org/10.5194/egusphere-2023-1564
Preprint. Discussion started: 13 July 2023

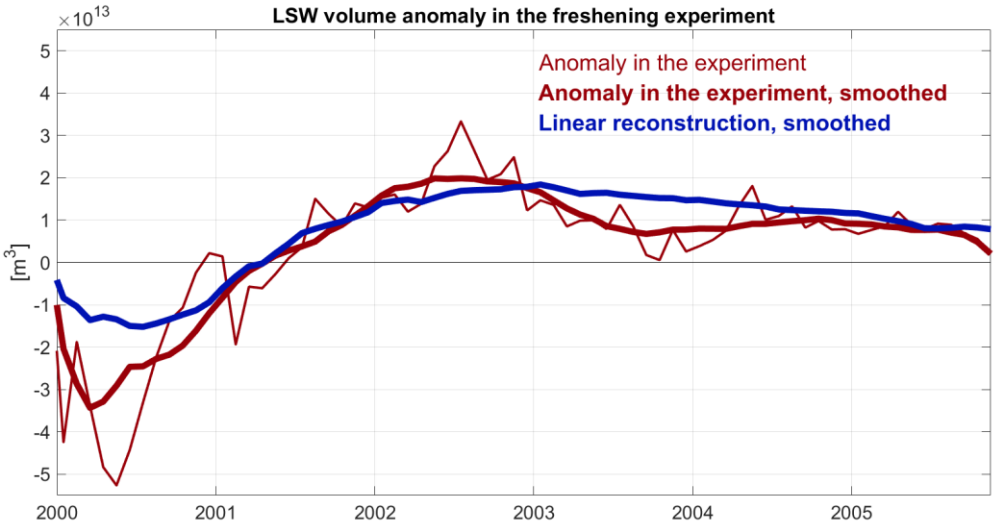

Figure E2: Time-evolving LSW volume anomaly [m^3] in the Labrador Sea in response to the freshwater flux perturbation pattern applied in January 2000 of the ECCO state estimate (thin red line) ; Same but smoothed with a 13-month running mean (thick red line) ; Linear reconstruction of the LSW volume anomaly in the perturbation experiment (thick blue line), also smoothed with a 13-month running mean.

Appendix F. Definition of regions analyzed in the study

We define the interior of the Labrador Sea as the part of the basin where the bottom depth reaches below 2.5 km (Fig. F1a). We also select a region north of 60ºN and west of 30ºW, encompassing the western part of the Irminger Sea and the southeast Greenland Shelf as illustrated in Fig. F1b.

We furthermore define an NAC pathway region as the area bounded by the -0.75 cm and -0.35 cm climatological SSH contours between 50°W and 30°W, and between 40°N and 58°N in the North Atlantic (Fig. F1c). The NAC flows northeastward across this region.

https://doi.org/10.5194/egusphere-2023-1564
Preprint. Discussion started: 13 July 2023

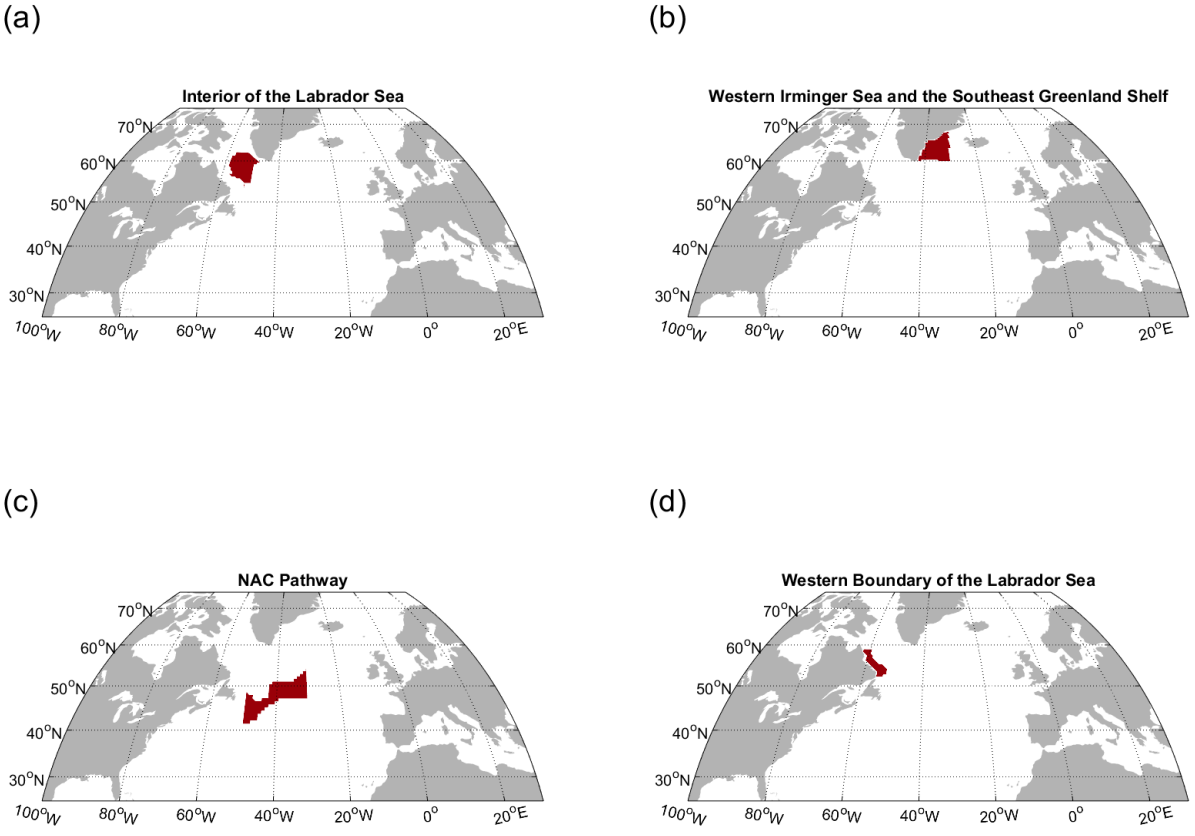

635

Figure F1: Spatial masks (red shading) of the regions defined in Appendix F: (a) the Labradro Sea interior; (b) the western Irminger Sea and the southeast Greenalnd Shelf; (c) the NAC pathway region; the Western Boundary of the Labrador Sea. The masks are set to 1 in the regions of interest and 0 everywhere else.

Finally, we define a Labrador Sea Western Boundary region as the basin area with a depth shallower than 2 km and
640 located south of 59°N (Fig. F1d).

In Fig. 10, we consider the preferred lead times at which the regions in Fig. F1 contribute to intermonthly variability in LSW volume. In comparison, in Fig. F2, we consider the preferred lead times in the contributions to interannual LSW variability.

645

https://doi.org/10.5194/egusphere-2023-1564
Preprint. Discussion started: 13 July 2023

650

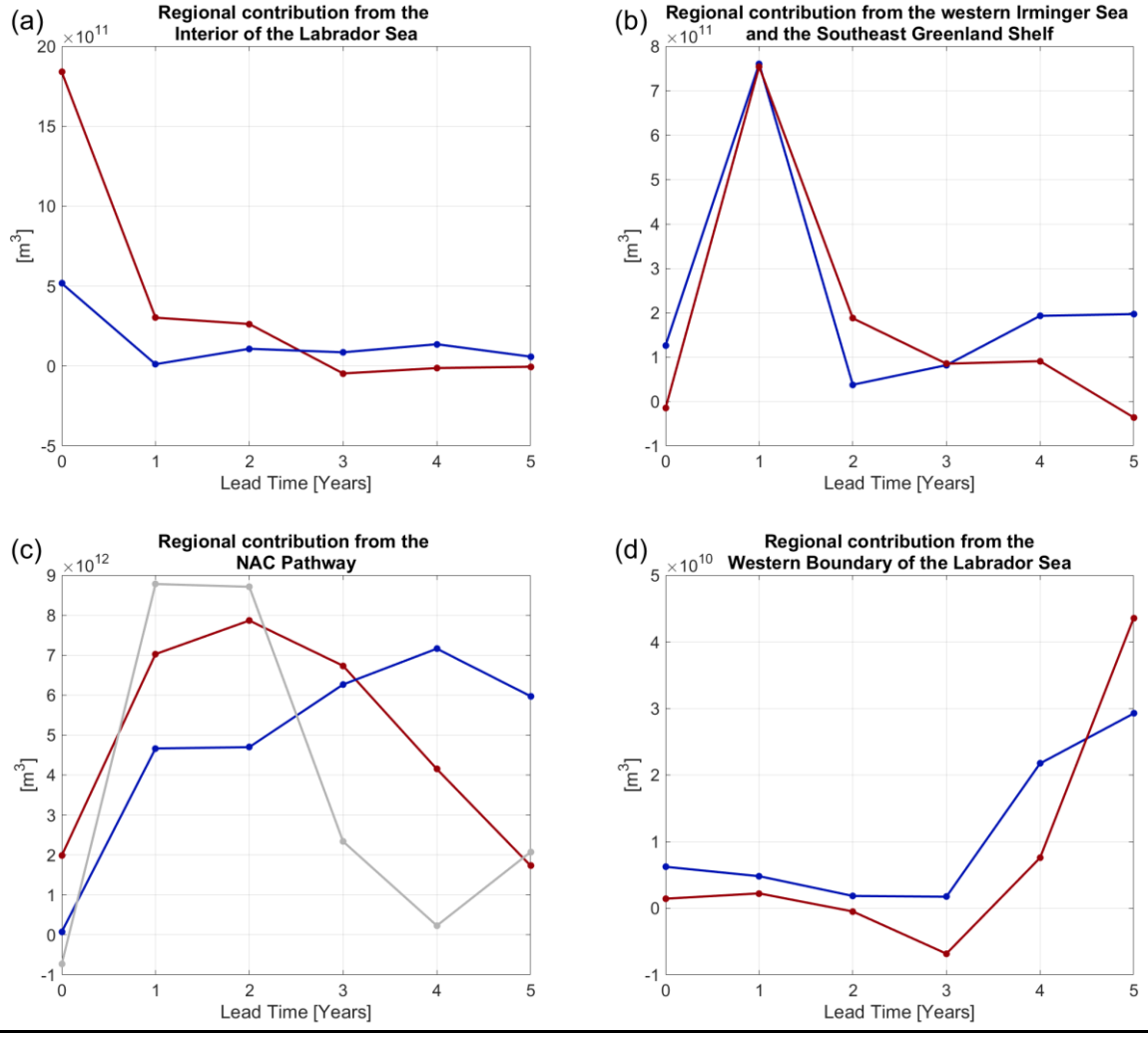

655 **Figure F2: Same as Fig. 10 but for regional contributions to interannual variability. Preferred lead times in the regional contributions of surface boundary conditions of LSW variability $[m^3]$, Eq. (11) over (a) the Labrador Sea interior (the region with bottom depth larger than 2.5 km, as shown in Fig. F1a; (b) the western part of the Irminger Sea and the southeast Greenland shelf (region shown in Fig. F1b); (c) the NAC pathway over the region defined in Appendix F and Fig. F1c; and (d) Labrador Sea Western Boundary, defined as the area shallower than 2 km and south of 59°N (as in Fig. F1d). The horizontal axis denotes the lead time.**
660 **Shown are the regional contributions of surface heat fluxes (red), freshwater fluxes (blue), and zonal wind stress (gray, panel b only) to interannual variability in LSW volume. Only sensitivity patterns from spring 2006 – winter 2007 objective functions are used in the calculation.**

https://doi.org/10.5194/egusphere-2023-1564
Preprint. Discussion started: 13 July 2023

Acknowledgements

We thank the ECCO, OSNAP, SNAP-DRAGON, and TICTOC research groups for the helpful discussions. The numerical simulations used in this study were conducted on the ARCHER2 supercomputer. We express our appreciation to the group that perpetually maintains the ECCO state estimate. We also thank Ralf Giering from FastOpt for the algorithmic differentiation software TAF. The color map vik (Crameri 2018) is applied in this study to provide accessibility to readers with color-vision deficiencies (Crameri et al., 2020). YK and MJM were funded by NERC TICTOC grant NE/P019064/1 and NERC BLT grant NE/S001433/1. HM was funded by the French National Center for Scientific Research (CNRS). DPM was supported by SNAP-DRAGON grant NE/T013494/1 and TICTOC grant NE/P019218/1. HLJ acknowledges SNAP-DRAGON grant NE/T013494/1 and WISHBONE grant (NE/T013451/1).

Declarations

The authors declare no competing interests.

Author contributions

All authors contributed to the conception, development, design, and writing of this study.

Data availability

All authors contributed to the conception, development, design, and writing of this study. The MITgcm code is available at https://github.com/MITgcm/. The ECCO state estimate model configuration is accessible at https://github.com/gaelforget/ECCOv4. ECCO's initial and boundary conditions are made available at https://web.corral.tacc.utexas.edu/OceanProjects/ECCO/ECCOv4. TAF is a proprietary algorithmic differentiation software provided by FastOpt. The scripts used to analyze data are available from the corresponding author upon a reasonable request.

References

Boland, E. J. D., Jones, D. C., Meijers, A. J. S., Forget, G., & Josey, S. A. (2021). Local and remote influences on the heat content of Southern Ocean mode water formation regions. *Journal of Geophysical Research: Oceans*, 126, e2020JC016585. https://doi.org/10.1029/2020JC016585

https://doi.org/10.5194/egusphere-2023-1564
Preprint. Discussion started: 13 July 2023

690 Brambilla, E., Talley, L. D., and Robbins, P. E. (2008), Subpolar Mode Water in the northeastern Atlantic: 2. Origin and transformation, *J. Geophys. Res.*, 113, C04026, doi:10.1029/2006JC004063.

Crameri, F. (2018) Scientific colour maps. *Zenodo*. http://doi.org/10.5281/zenodo.1243862

695 Crameri, F., G.E. Shephard, and P.J. Heron (2020) The misuse of colour in science communication, *Nature Communications*, 11, 5444. doi: 10.1038/s41467-020-19160-7

Desbruyères, D. G., E. L. McDonagh, B. A. King, F. K. Garry, A. T. Blaker,B. I. Moat, and H. Mercier (2014), Full-depth temperature trends in the northeastern Atlantic through the early 21st century, *Geophys. Res. Lett.*, *41*, 7971–7979,
700 doi:10.1002/2014GL061844.

Florindo-López, C., S. Bacon, Y. Aksenov, L. Chafik, E. Colbourne, and N. P. Holliday, 2020: Arctic Ocean and Hudson Bay Freshwater Exports: New Estimates from Seven Decades of Hydrographic Surveys on the Labrador Shelf. *J. Climate*, **33**, 8849–8868, https://doi.org/10.1175/JCLI-D-19-0083.1.

705

Forget, G., J.M. Campin, P. Heimbach, C.N. Hill, R.M. Ponte, and C. Wunsch, 2015: ECCO version 4: an integrated framework for non-linear inverse modeling and global ocean state estimation. Geosci. Model Dev., 8, 3071-3104. https://doi.org/10.5194/gmd-8-3071-2015

710 Giering, R., 2010: Transformation of algorithms in Fortran Version 1.15 (TAF Version 1.9.70). FastOpt.

Fukumori, I., O. Wang, I. Fenty, G. Forget, P. Heimbach, and R. M. Ponte, 2017: ECCO Version 4 Release 3, http://hdl.handle.net/1721.1/110380, doi:1721.1/110380.

715 Hakkinen, S., and P. B. Rhines (2009), Shifting surface currents in the northern North Atlantic Ocean, J. Geophys. Res., 114, C04005, doi:10.1029/2008JC004883.

Heimbach, P., Wunsch, C., Ponte, R. M., Forget, G., Hill, C., & Utke, J. (2011). Timescales and regions of the sensitivity of Atlantic meridional volume and heat transport: Toward observing system design. Deep Sea Research Part II: Topical Studies
720 in Oceanography, 58, 1858–1879. https://doi.org/10.1016/j.dsr2.2010.10.065

Holliday, N.P., Bersch, M., Berx, B. *et al.* Ocean circulation causes the largest freshening event for 120 years in eastern subpolar North Atlantic. *Nat Commun* **11**, 585 (2020). https://doi.org/10.1038/s41467-020-14474-y

Houpert, L., Inall, M. E., Dumont, E., Gary, S., Johnson, C., Porter, M., et al. (2018). Structure and transport of the north atlantic current in the Eastern Subpolar Gyre from sustained glider observations. *Journal of Geophysical Research: Oceans*, 123, 6019– 6038. https://doi.org/10.1029/2018JC014162

Jones, D. C., Forget, G., Sinha, B., Josey, S. A., Boland, E. J. D., Meijers, A. J. S., et al. (2018). Local and remote influences on the heat content of the Labrador sea: an adjoint sensitivity study. *J. Geophys. Res. Oceans* **123**, 2646–2667. doi: 10.1002/2018JC013774

Jutras, M., Dufour, C.O., Mucci, A. *et al.* Large-scale control of the retroflection of the Labrador Current. *Nat Commun* **14**, 2623 (2023). https://doi.org/10.1038/s41467-023-38321-y

Koelling, J., Atamanchuk, D., Karstensen, J., Handmann, P., and Wallace, D. W. R. (2022) Oxygen export to the deep ocean following Labrador Sea Water formation, Biogeosciences, 19, 437–454, https://doi.org/10.5194/bg-19-437-2022

Kostov, Y., Johnson, H. L. & Marshall, D. P. AMOC sensitivity to surface buoyancy fluxes: the role of air–sea feedback mechanisms. (2019) Clim. Dyn. 53, 4521–4537. DOI: https://doi.org/10.1007/s00382-019-04802-4

Kostov, Y., Johnson, H.L., Marshall, D.P. *et al.* Distinct sources of interannual subtropical and subpolar Atlantic overturning variability. (2021) *Nat. Geosci.* **14,** 491–495. doi: https://doi.org/10.1038/s41561-021-00759-4

Kostov, Y., Messias, MJ., Mercier, H. *et al.* Fast mechanisms linking the Labrador Sea with subtropical Atlantic overturning. *Clim Dyn* (2022). https://doi.org/10.1007/s00382-022-06459-y

Lazier, J., R. Hendry, A. Clarke, I. Yashayaev, P. Rhines (2002)Convection and restratification in the Labrador Sea, 1990–2000 Deep Sea Res. Oceanogr. Res. Pap., 49 (10), pp. 1819-1835, 10.1016/S0967-0637(02)00064-X

Li, Feili, M. Susan Lozier, Gokhan Danabasoglu, Naomi P. Holliday, Young-Oh Kwon, Anastasia Romanou, Steve G. Yeager, and Rong Zhang. "Local and Downstream Relationships between Labrador Sea Water Volume and North Atlantic Meridional Overturning Circulation Variability", Journal of Climate 32, 13 (2019): 3883-3898, doi: https://doi.org/10.1175/JCLI-D-18-0735.1

Loose, N., Heimbach, P., Pillar, H. R., & Nisancioglu, K. H. (2020). Quantifying dynamical proxy potential through shared adjustment physics in the North Atlantic. Journal of Geophysical Research: Oceans, 125, e2020JC016112. https://doi.org/10.1029/2020JC016112

https://doi.org/10.5194/egusphere-2023-1564
Preprint. Discussion started: 13 July 2023

Lozier S.M., Gary S.F., Bower A.S. (2012) Simulated pathways of the overflow waters in the North Atlantic: Subpolar to subtropical export Deep-Sea Res. II, 85, pp. 147-153, 10.1016/j.dsr2.2012.07.037

Lozier et al. (2017). Overturning in the Subpolar North Atlantic Program: A New International Ocean Observing System, *Bulletin of the American Meteorological Society*, 98(4), 737-752. DOI: https://doi.org/10.1175/BAMS-D-16-0057.1

Mackay, Neill, Chris Wilson, Jan Zika, and N. Penny Holliday. "A Regional Thermohaline Inverse Method for Estimating Circulation and Mixing in the Arctic and Subpolar North Atlantic", Journal of Atmospheric and Oceanic Technology 35, 12 (2018): 2383-2403, doi: https://doi.org/10.1175/JTECH-D-17-0198.1

Mackay, N. S., Wilson, C., Holliday, P., Zika, J. D., 2020: The observation-based application of a Regional Thermohaline Inverse Method to diagnose the formation and transformation of Labrador Sea water from 2013-2015. *Journal of Physical Oceanography*, 50, 1533–1555. DOI: https://doi.org/10.1175/JPO-D-19-0188.1

Marshall, J., Hill, C., Perelman, L., and Adcroft, A. (1997), Hydrostatic, quasi-hydrostatic, and nonhydrostatic ocean modeling, J. Geophys. Res., 102(C3), 5733– 5752, doi:10.1029/96JC02776.

Marotzke, J., Giering, R., Zhang, K. Q., Stammer, D., Hill, C., and Lee, T. (1999), Construction of the adjoint MIT ocean general circulation model and application to Atlantic heat transport sensitivity, J. Geophys. Res., 104(C12), 29529– 29547, doi:10.1029/1999JC900236.

Messias, MJ., Mercier, H. The redistribution of anthropogenic excess heat is a key driver of warming in the North Atlantic. *Commun Earth Environ* **3**, 118 (2022). https://doi.org/10.1038/s43247-022-00443-4

Oldenburg, D., D., Wills, R. C. J., Armour, K. C., Thompson, L., Jackson, L. C. (2021). Mechanisms of Low-Frequency Variability in North Atlantic Ocean Heat Transport and AMOC, Journal of Climate, 34(12), 4733-4755. https://doi.org/10.1175/JCLI-D-20-0614.1

Pérez, F. F., Mercier, H., Vázquez-Rodríguez, M., Lherminier, P., Velo, A., Pardo, P. C., et al. (2013). Atlantic Ocean CO2 uptake reduced by weakening of the meridional overturning circulation. *Nature Geoscience*, 6(2), 146–152. https://doi.org/10.1038/ngeo1680

https://doi.org/10.5194/egusphere-2023-1564
Preprint. Discussion started: 13 July 2023

Petit, T., Lozier, M. S., Josey, S. A., & Cunningham, S. A. (2020). Atlantic deep water formation occurs primarily in the Iceland Basin and Irminger Sea by local buoyancy forcing. Geophysical Research Letters, 47, doi: e2020GL091028. https://doi.org/10.1029/2020GL091028

795 Petit, T, M. S. Lozier , S. A. Josey, and S. A. Cunningham (2021) Role of air–sea fluxes and ocean surface density in the production of deep waters in the eastern subpolar gyre of the North Atlantic. Ocean Sci., 17, 1353–1365, https://doi.org/10.5194/os-17-1353-2021

Petit, T, J. Robson, D. Ferreira, & L. Jackson. (2022, submitted) Impact of resolution in the dense water formation over the
800 North Atlantic for a hierarchy of climate model HadGEM3, Journal of Advances in Modeling Earth System.

Pickart R.S., Straneo F., Moore G. (2003a) Is Labrador Sea Water formed in the Irminger basin? Deep Sea Res. Part I, 50 (1) (2003a), pp. 23-52, 10.1016/S0967-0637(02)00134-6

805 Pickart RS, Spall MA, Ribergaard MH, Moore GW, Milliff RF. (2003b) Deep convection in the Irminger Sea forced by the Greenland tip jet. Nature. Jul 10;424(6945):152-6. doi: 10.1038/nature01729.

Pillar, H., P. Heimbach, H. Johnson, and D. Marshall, 2016: Dynamical attribution of recent variability in Atlantic overturning. J. Climate, 29, 3339-3352, doi:https://doi.org/10.1175/JCLI-D-15-0727.1.

810

Raj RP, et al. Quantifying Atlantic Water transport to the Nordic Seas by remote sensing. *Remote Sens. Environ.* 2018;216:758–769. doi: 10.1016/j.rse.2018.04.055

Raj, R. P., Chatterjee, S., Bertino, L., Turiel, A., and Portabella, M.: The Arctic Front and its variability in the Norwegian Sea, Ocean Sci., 15, 1729–1744, https://doi.org/10.5194/os-15-1729-2019, 2019.

815

Rhein M, Steinfeldt R, Kieke D, Stendardo I, Yashayaev I. 2017 Ventilation variability of Labrador SeaWater and its impact on oxygen and anthropogenic carbon: a review. *Phil. Trans. R. Soc. A* **375**: 20160321. http://dx.doi.org/10.1098/rsta.2016.0321

Roussenov VM, Williams RG, Lozier MS, Holliday NP, Smith DM (2022) Historical reconstruction of subpolar North Atlantic
820 overturning and its relationship to density. *J Geophys Res* 127:32. https://doi.org/10.1029/2021JC017732

Smith, T. and P. Heimbach. 2019. Atmospheric origins of variability in the South Atlantic meridional overturning circulation. J. Clim., 32(5), 1483-1500, doi:10.1175/JCLI-D-18-0311.1.

https://doi.org/10.5194/egusphere-2023-1564
Preprint. Discussion started: 13 July 2023

Talley, L. D., and M. S. McCartney. "Distribution and Circulation of Labrador Sea Water", Journal of Physical Oceanography 12, 11 (1982): 1189-1205, doi: https://doi.org/10.1175/1520-0485(1982)012<1189:DACOLS>2.0.CO;2

Terenzi, F., Hall, T. M., Khatiwala, S., Rodehacke, C. B., and LeBel, D. A. (2007), Uptake of natural and anthropogenic carbon by the Labrador Sea, *Geophys. Res. Lett.*, 34, L06608, doi:10.1029/2006GL028543.

Våge, K., Pickart, R.S., Spall, M.A., Moore, G.W.K., Valdimarsson, H., Torres, D.J., Erofeeva, S.Y. and Nilsen, J.E.Ø. (2013) Revised circulation scheme north of the Denmark Strait. *Deep Sea Research Part I*, **79**, 20– 39. https://dx.doi.org/10.1016/j.dsr.2013.05.007

Weijer, W., T.W.N. Haine, A.H. Siddiqui, W. Cheng, M. Veneziani, and P. Kurtakoti. 2022. Interactions between the Arctic Mediterranean and the Atlantic Meridional Overturning Circulation: A review. Oceanography 35(3–4):118–127, https://doi.org/10.5670/oceanog.2022.130.

Yashayaev, I., Bersch, M., and van Aken, H. M. (2007a), Spreading of the Labrador Sea Water to the Irminger and Iceland basins, *Geophys. Res. Lett.*, 34, L10602, doi:10.1029/2006GL028999.

Yashayaev, I., van Aken, H. M., Holliday, N. P., and Bersch, M. (2007b), Transformation of the Labrador Sea Water in the subpolar North Atlantic, *Geophys. Res. Lett.*, 34, L22605, doi:10.1029/2007GL031812.

Yashayaev, I., and Loder, J. W. (2009), Enhanced production of Labrador Sea Water in 2008, *Geophys. Res. Lett.*, 36, L01606, doi:10.1029/2008GL036162.

Yeager, S., F. Castruccio, P. Chang, G. Danabasoglu, E. Maroon, J. Small, H. Wang, L. Wu, S. Zhang (2021) An outsized role for the Labrador Sea in the multidecadal variability of the Atlantic overturning circulation. Sci. Adv. 7, eabh3592. DOI: 10.1126/sciadv.abh3592

Zhao, J., Bower, A., Yang, J. et al. (2018) Meridional heat transport variability induced by mesoscale processes in the subpolar North Atlantic. *Nat Commun* 9, 1124. https://doi.org/10.1038/s41467-018-03134-x

Zou, S., Lozier, M. S., 2016, Breaking the linkage between Labrador Sea Water production and its advective export to the subtropical gyre. J. Phys. Oceanogr. 46, 2169–2182. doi:10.1175/JPO-D-15-0210.1